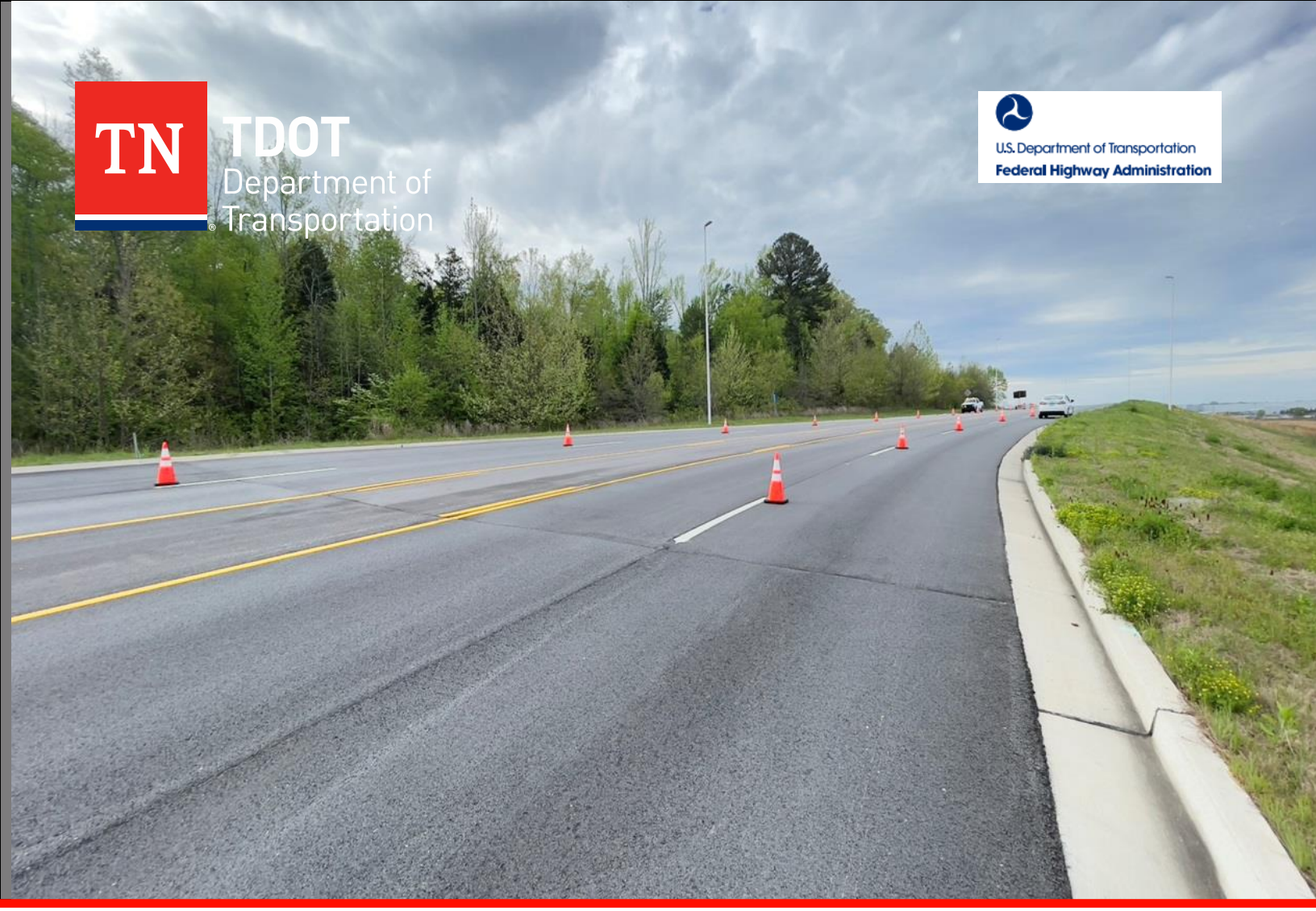

Field Performance Testing and Evaluation of the Constructed Inverted Pavements in Tennessee

Research Final Report from University of Tennessee, Knoxville | Guantao Cheng, Kai Huang, Baoshan Huang) | May 31, 2024

Sponsored by Tennessee Department of Transportation Long Range Planning

Research Office & Federal Highway Administration

DISCLAIMER

This research was funded through the State Planning and Research (SPR) Program by the Tennessee Department of Transportation and the Federal Highway Administration under RES2023-26*:* Field Performance Testing and Evaluation of the Constructed Inverted Pavements in Tennessee .

Technical Report Documentation Page

1. Report No. RES 2023-26	2. Government Accession No.	3. Recipient's Catalog No.
4. Title and Subtitle *Field Performance Testing and Evaluation of the Constructed Inverted Pavements in Tennessee*		5. Report Date May 2024 6. Performing Organization Code
7. Author(s) Guantao Cheng, Kai Huang, Baoshan Huang		8. Performing Organization Report No.
9. Performing Organization Name and Address The University of Tennessee, Knoxville 851 Neyland Drive Knoxville, TN, 37996		10. Work Unit No. (TRAIS) 11. Contract or Grant No. RES 2023-26
12. Sponsoring Agency Name and Address Tennessee Department of Transportation 505 Deaderick Street, Suite 900 Nashville, TN 37243		13. Type of Report and Period Covered Final report December 2022 – May 2024 14. Sponsoring Agency Code
15. Supplementary Notes Conducted in cooperation with the U.S. Department of Transportation, Federal Highway Administration.		

16. Abstract

The Tennessee Department of Transportation (TDOT) has been exploring inverted pavement technology for its potential for significant cost benefits compared to conventional flexible pavement. This research, initiated due to TDOT's interest in the potential cost and performance advantages of inverted pavement yet cautious about its statewide implementation without thorough validation, has led to in-depth findings. A previous study (RES2020-12) demonstrated that inverted pavements exhibit enhanced resistance to cracking and deformation. This research conducted a comprehensive assessment and evaluation of a test section in Chattanooga, constructed as an industrial service road for Volkswagen, allowing for an in-depth engagement from construction through to the operational phase. This setup facilitated direct data collection and analysis, comparing the performance of inverted pavement structures against conventional pavements under the same traffic and environmental conditions. Despite the limited time frame, which did not allow the appearance of significant signs of distress, the research team employed AASHTOWare Pavement ME software for performance prediction and cost analysis of both pavement types. This was supported by rigorous testing methodologies, including Ground Penetration Radar (GPR) scanning, Falling Weight Deflectometer (FWD) measurements, and field coring to ensure the accuracy and reliability of the predictive analysis. The research further implemented ride quality assessments using the Mean Roughness Index (MRI) and conducted a detailed cost analysis using the Estimated Uniform Annual Cost (EUAC) formula. These analyses revealed that inverted pavements, despite their relatively thinner layers, could offer equivalent performance and better cost-efficiency, thus presenting a viable alternative to conventional pavement structures. The findings advocate for the potential wider adoption of inverted pavement technology in Tennessee, underlining its durability, cost savings, and environmental sustainability advantages.

17. Key Words Inverted pavement; performance monitoring; performance predictions; cost benefits; Falling Weight Deflectometer; ride quality.	18. Distribution Statement No restriction. This document is available to the public from the sponsoring agency at the website http://www.tn.gov/.

19. Security Classif. (of this report) Unclassified	20. Security Classif. (of this page) Unclassified	21. No. of Pages	22. Price

Acknowledgment

We would like to thank the Tennessee Department of Transportation (TDOT) for funding this research project. We have maintained a close collaboration with regional engineers and local technicians, whose invaluable support has been crucial in advancing our research objectives. Without their support, completing this research project would not have been feasible. We would also like to thank the administrative staff from the TDOT Research Office who have worked very closely with our research team and kept the whole project on the proposed schedule.

Executive Summary

The Tennessee Department of Transportation (TDOT) has been exploring inverted pavement technology for its potential for significant cost and environmental benefits but has hesitated to widely implement it in the state due to the need for more rigorous demonstration. The University of Tennessee, Knoxville (UTK), conducted a study (RES2020-12) that revealed the superiority of inverted pavement over conventional flexible pavement in terms of performance under the same conditions, based on tests at the Vulcan Materials Company in Knoxville and further full-scale testing at UTK. The inverted pavements showed better resistance to cracking and deformation. The recent TDOT research project established a test inverted pavement section in Chattanooga, allowing the research team extensive involvement in all construction phases for direct data collection and analysis. Constructed as an industrial service road for Volkswagen, this project allowed comprehensive engagement from construction to service, conducting detailed comparisons of the performance of inverted sections against conventional sections under identical traffic and environmental conditions after a two-year service for the heavy trucks.

Since no significant distress has been observed in the test pavement sections due to a short in-service period, the research team employed AASHTOWare Pavement ME software to predict the pavement performance and conducted a cost analysis for both the inverted and conventional sections. To ensure the accuracy and reliability of the predictions and analysis, comprehensive tests and analysis were extensively conducted, encompassing reviewing the design documents, Ground Penetration Radar (GPR) scanning, Falling Weight Deflectometer (FWD) measurements, and field coring tests.

The ride quality can still be accurately assessed even without visible signs of distress of recently constructed pavements. The research team conducted a detailed assessment of roughness for both conventional and inverted pavement sections, utilizing continuous Mean Roughness Index (MRI) data to quantify ride quality. The measured MRI values are benchmarked against federal roughness thresholds, highlighting the better condition of most inverted sections.

The precise thickness and modulus of structure layers served as crucial inputs for Pavement ME software, which was meticulously verified to ensure the accuracy of current conditions in relation to the design specifications. Ground Penetrating Radar (GPR) and field coring were employed to determine the consistency of the thickness of constructed layers with the design specifications. The consistency of GPR results and coring measurements compared with the design thicknesses allowed the research team to proceed confidently to subsequent analysis. The laboratory tests for resilient modulus were crucial in validating the back-calculated modulus values. Two distinct FWD tests were carried out: one before applying the paving surface and another after a year of heavy traffic exposure. Considering the first FWD was conducted before the surface layer was paved, the research team chose to use the back-calculated modulus of the structure layers based on the second FWD data conducted on the completed pavement sections to provide a robust basis for analysis.

The research team used Pavement ME software to validate the cost benefits of inverted pavement for performance prediction and preliminary cost analysis based on the laboratory and field data verified input data. Since the Pavement ME software does not include the design type and settings specifically for the inverted pavement configuration, the research team used an

equivalent layer to represent both the CTB layer and the subgrade. This method allows the inverted pavement structure to be simulated within the software like traditional flexible pavement with a relatively stiffer equivalent subgrade since it equivalently combines the CTB layer and subgrade. Its equivalent resilient modulus is back-calculated using FWD data via the BAKFAA software. Meanwhile, the climate data was meticulously sourced from the Pavement ME website to ensure the model reflects realistic environmental conditions. For cost-effectiveness comparison, the research applied the Estimated Uniform Annual Cost (EUAC) formula, using a 4% discount rate and recent bidding data for material costs. Prices for asphalt concrete, aggregate base layer, and Cement Treated Base (CTB) were derived from local cost data, providing a detailed financial analysis of both conventional and inverted pavement sections.

Key Findings

- The preliminary evaluations using Deflection basin parameters (DBP) for conventional and inverted pavement sections indicate both types of pavements were rated between 'very good' and 'good'. The Surface Crack Index (SCI) values for the inverted pavement were higher than those for the conventional pavement due to the thickness differences in the asphalt concrete (AC) layer, given the AC layer in the inverted pavement is much thinner than that in the conventional pavement.
- The measured Mean Roughness Index (MRI) showed both conventional and inverted sections exhibited good performance in surface roughness, in which three of the tested inverted lane sections achieved a "Very Good" rating, with only one section rated as "Good". For conventional pavement sections, two tested lane sections were rated "Good", while the others were rated "Very Good". The conventional pavement showed a higher discrepancy in roughness, suggesting that inverted pavement may maintain surface roughness more effectively under certain traffic conditions.
- The AASHTOWare ME Design software results showed minor distress level differences between the conventional and inverted sections, except for thermal cracking. Both types of pavements were predicted to perform well, staying within acceptable limits for IRI, rutting depth, bottom-up cracking, and not reaching failure thresholds. The conventional pavement showed slightly better performance after 20 years. No significant bottom-up cracking was seen in both types. However, the conventional pavement had substantially less thermal cracking than the inverted pavement because thicker asphalt layers can lessen thermal cracking. Both pavement types are expected to last 20 years without significant failure. It is worth noting that the AC layer's inverted pavement thickness is only ¼ of the conventional one.
- Through cost analysis, the EUAC for inverted pavements is determined to be 21,591 US dollars, compared to 24,725 US dollars for conventional pavements, reflecting a 14.52% cost saving. This indicates that the test inverted pavement is more cost-efficient than the test conventional pavement section under similar pavement performance.

Key Recommendations

- The inverted pavement structure demonstrated equivalent performance compared to the conventional flexible pavement structure under the same loading and environmental

conditions, with a 14.52% cost saving. This evidence positions inverted pavement as a viable alternative to conventional flexible pavement.

- The Chattanooga test pavement sections have been operational for two years and have yet to show significant signs of distress. Thus, this project has utilized the Pavement ME software for predicting service life and conducting cost analysis. Thorough and continuous distress monitoring and precise measurements will provide accurate and realistic data on the performance of both pavement types, enhancing the reliability of cost-benefit comparisons and supporting the confident adoption of inverted pavement across the state. Therefore, continuous engagement of TDOT and the research team is strongly recommended in monitoring and conducting comparative assessments of the performance on Chattanooga test pavements beyond this project.
- In pursuit of carbon neutrality, evaluating and comparing the carbon footprint of both conventional and inverted pavements is imperative. The primary sources of carbon emissions—production and transportation of asphalt mixtures, aggregates, and cement—highlight the environmental impact of pavement construction. Using a thinner asphalt layer in inverted pavements presents a significant opportunity to reduce carbon emissions. Therefore, carbon footprint analysis is advocated to promote the sustainable development of the state's transportation infrastructure.
- A comprehensive design and sensitivity analysis for inverted/inverted comparison, considering cost-benefit and carbon footprint benchmarks, is beneficial for better inverted pavement performance. While inverted pavements have proven their durability and performance against conventional pavements under similar conditions, optimizing their structure and material comparison of different inverted pavement designs remains crucial. Such analysis will ensure the best possible performance of inverted pavements, supporting further implementation across the state.

Table of Contents

List of Tables

List of Figures

Chapter 1 Introduction

1.1 Problem Statement

Tennessee Department of Transportation (TDOT) has long been trying to initiate and adopt inverted pavement technology due to its significant cost benefits. Over the past several years, TDOT has shown interest in implementing the inverted pavement technique on more road projects in the state. Despite this enthusiasm, the push has not progressed beyond the letting stage, primarily due to a lack of confidence in the technology. The University of Tennessee (UT), Knoxville, recently conducted a TDOT research project (RES2020-12) addressing the performance of inverted pavement. Based on the test section in the Vulcan Materials Company in Knoxville, the inverted pavement structure outperformed the conventional flexible pavement under the same loading, temperature, and environmental conditions after a two-year service for heavy trucks. The field investigation utilized a Falling Weight Deflectometer (FWD), ground penetrating radar (GPR), Benkelman beam, and 3-D laser road profile test. In addition, full-scale inverted pavement tests using an Accelerated Pavement Tester (APT) have also been conducted at the UT campus. The test results showed that the inverted pavement structure performed better in cracking and permanent deformation.

The latest TDOT research project constructed a test section in Chattanooga. The test section enabled the research team to be deeply involved in every construction phase, allowing for the direct collection and analysis of data throughout the process. The Chattanooga inverted pavement project was built as an industrial service road for the Volkswagen Company. The primary objective of this proposed research is to monitor and evaluate the short- and long-term performance, longevity, and cost-effectiveness of the inverted and conventional pavement test sections in Chattanooga. The performance comparison of inverted and conventional sections aims to provide evidence that inverted pavement can serve as an ideal alternative pavement structure in Tennessee. A field investigation was conducted in Ferdinand Piech Hwy, Chattanooga to achieve this. Non-destructive testing methods such as ground penetration radar (GPR) and falling weight deflectometer (FWD) were used to assess the pavement structures' actual thickness and surface conditions. The field coring for both pavement sections allows the research team to retrieve base materials for laboratory tests, measure the different pavement layer thicknesses, and verify the information provided by the as-built plans. This study's key findings and recommendations present a better understanding of the inverted pavement structure.

1.2 Objectives

The proposed research's primary goal is to comprehensively assess both the short-term and long-term performance, durability, and cost-effectiveness of both inverted and conventional pavement test sections established in Chattanooga. A thorough review of design documents and the verification of various tests and measurements conducted on the Chattanooga test sections aims to generate reliable inputs for precise pavement performance predictions. This comprehensive analysis aims to provide valuable insights into the operational efficiencies and lifecycle costs associated with inverted pavements compared to traditional approaches. This in-depth analysis is expected to provide valuable insights into the operational efficiencies and

lifecycle costs of inverted pavement compared to conventional methods. By evaluating short-term effects and projecting long-term performance, the research will provide a robust foundation of evidence on the suitability of inverted pavement as a preferred alternative for future roadway construction projects within the state.

1.3 Report organization

The report is organized as follows: Chapter 2 provides a comprehensive review of the characteristics and development of inverted pavements, including an examination of relevant fields and laboratory investigations of such pavements. Chapter 3 outlines the methodology to achieve the project's goals, including field and experimental procedures for assessing material properties and pavement performance. Chapter 4 presents findings from the pavement database analysis, experimental results, and lifecycle cost/benefit analysis of inverted pavement. Finally, Chapter 5 wraps up the study, providing conclusions and recommendations from the project's outcomes.

Chapter 2 Literature Review

2.1 Inverted Pavements

The inverted pavement system, first introduced in South Africa during the 1950s (Cortes and Santamarina, 2013), stands out as a promising, cost-effective alternative to traditional flexible pavement, relying on its durability and cost-effectiveness. Unlike conventional pavement, where a thicker asphalt layer sits atop a granular base, inverted pavement systems consist of a thin asphalt concrete (AC) layer for the surfacing, a high-quality unbound aggregate base (UAB), and a stiffer cement-treated base (CTB). The term 'inverted' indicates that the sequence of pavement layers is different, and the stiffness and strength of its layers do not decrease with pavement depth. Lewis et al. (2012) adopted the term 'sandwiched pavement' to describe the arrangement of layer stiffness in the pavement, which resembles a sandwich structure with a UAB layer with lower stiffness placed between the AC and CTB layers. A key aspect of inverted pavement is the stress-dependent properties of the filling of the sandwich, the UAB layer, within the inverted configuration. The stiffness of the UAB layer adapts to loading conditions, achieving greater stiffness as the density and confinement of the granular layer increases under the influence of repetitive traffic loads.

As traffic volume grows and pavement engineering evolves, there's a pressing need for more efficient and high-performing pavement solutions within tight budget constraints faced by transportation departments. With their thick asphalt layers, traditional pavements deplete natural resources like aggregates and pollute the air (Khare et al., 2020). The inverted pavement system with a unique feature of thinner asphalt layers without sacrificing performance is essential for extending pavement lifespan and enhancing structure efficiency. Inverted pavement structures have emerged as a viable and sustainable option, promising to minimize these performance and environmental issues when assessed through life cycle assessment (LCA) methods (Papadopoulos and Santamarina, 2016, 2019; US DOT, 2017).

2.2 Field and Laboratory Investigation of Inverted Pavements

Initial laboratory experiments and field investigations explored this reverse structure's durability and load support in recent years. Inverted pavement design showed greater rutting and fatigue resistance than traditional flexible pavements (Baghel et al. 2021). A full-scale inverted pavement project was constructed and tested in Morgan County and LaGrange Bypass in Georgia, USA (Lewis et al. 2012). The field studies comparing rutting and cracking between inverted and conventional pavement sections revealed that the inverted sections performed well and were cost-effective. Cortes and Santamarina (2013) provided a macro-scale analysis and preliminary numerical studies on the LaGrange Bypass inverted pavement, highlighting that the nonlinear stiffness of UAB in inverted structures is the key characteristic to enhancing understanding of inverted pavement behavior. Ghanizadeh et al. (2022) discussed that the quality of granular materials for UAB is essential to secure the enhanced performance of inverted pavement systems. Jiang et al. (2022) conducted a detailed field investigation and numerical analysis on an inverted pavement system in Tennessee, USA, presenting a performance comparison between an inverted pavement section and a conventional section. The study clarified and simulated the nonlinear stress dependency of the UAB within the

inverted pavement structure. Biswal et al. (2020) studied the structural behavior of inverted pavement, considering the isotropic and anisotropic characteristics of UAB. Numerical simulations such as Finite Element Method (FEM) were adopted to model and illustrate the characteristics of the inverted pavements (Cortes and Santamarina, 2013, Papadopoulos and Santamarina, 2016, 2019). The numerical results showed that the AC layer in the inverted configuration developed a lower level of tensile strain, thus resulting in a longer fatigue life (Papadopoulos and Santamarina, 2016). A comparative study between the inverted and conventional pavements was performed using the nonlinear simulation approach in ABAQUS FEM software (Jiang et al. 2021). These studies aimed to demonstrate that inverted pavement is an ideal alternative to conventional flexible pavement due to its good performance and economic efficiency.

Donovan (2022) employed mechanistic-empirical (ME) pavement analysis software to compare inverted and conventional pavements. These analyses indicated that many inverted designs outperformed conventional ones despite having a thinner AC layer. Further advancements were made by considering the economic and environmental aspects. Inverted pavements were more cost-effective, requiring less asphalt and other materials, reducing construction costs and environmental impact (Plati, 2019). The evolution of inverted pavement is marked by continuous research and adaptation. With advancements in material sciences and construction technologies, inverted pavement has become a more prevalent choice in certain contexts. Its development reflects a growing awareness of the need for sustainable, cost-effective, and durable road infrastructure (Plati, 2019). This shift was also influenced by the accumulating evidence from different regions, notably South Africa, Brazil (Almeida, 2021), and the USA, where inverted base pavements were extensively studied. In recent years, the inverted pavement design has continued to evolve, integrating modern technologies and materials to enhance its performance further. The focus has been optimizing the design for specific environmental conditions and traffic patterns, ensuring that this innovative pavement structure meets contemporary road infrastructure's diverse needs.

Various field investigations on inverted pavement structures have been conducted to explore more cost-effective and durable materials used in inverted configurations. Khan et al. (2022) presented laboratory and field performance results for an inverted pavement system. This study tested and verified that fly ash can replace some common aggregate needed for pavement construction, aiming to reduce construction costs. Papadopoulos and Santamarina (2019) explored the feasibility of using geocell reinforcement in lower-quality materials for inverted pavement systems. It found that geocell reinforcement of the granular base layer significantly improved fatigue and rutting performances, presenting a viable alternative in scenarios where premium quality materials are unavailable. Jiang et al. (2024) conducted a detailed analysis of full-scale inverted pavements and evaluated the effectiveness of geogrid reinforcement on rutting resistance. Their findings suggest that incorporating geogrid into the UAB layer significantly enhances its ability to resist rutting. The most effective placement of the geogrid is identified to be in the upper third of the UAB layer for optimal performance improvements.

Chapter 3 Methodology

3.1 Ground Penetration Radar (GPR)

Ground Penetrating Radar (GPR) is a non-invasive geophysical method that uses radar pulses to image the subsurface. This technology operates by emitting a pulse of electromagnetic energy into the ground through a radar transmitter. As these waves travel through the subsurface, they encounter different materials and buried objects with varying electrical properties. When a wave encounters a material boundary or object with contrasting dielectric permittivity, part of the energy is reflected to the surface while the rest penetrates deeper. A radar receiver then detects these reflected signals. The time delay between the emission and reception of the pulse is measured and used to estimate the object's depth or material boundary. The strength of the returning pulse provides information on the nature of the subsurface objects or layers. GPR can detect various materials, including rock, soil, ice, fresh water, pavements, and voids. By analyzing the patterns and strength of the reflected radar signals, GPR can create images or profiles of the subsurface, revealing buried structures, utilities, and anomalies without any physical excavation (Jol, 2008).

Figure 3-1. Pavement thickness detection process using GPR on the investigated pavement section in Chattanooga, TN.

The research team used a GSSI SIR 4000 GPR antenna (350 MHz) along with a three-wheel cart for this project. The general setup is shown in Figure 3-1. The applicable tested areas are limited from the lane center line to the outer wheel pass (OWP). The GPR results were exported and analyzed using GSSI RADAN 7 software. Two paths spanning the construction boundaries between conventional and inverted pavements were selected for GPR scanning and analysis, as shown in Figure 3-2. According to the documentation of the previous research project (No. RES 2020-12, Jiang et al. 2022) and the TDOT design document (CNU221-Typical Section), the layer configuration of conventional pavement section in this study was constructed as asphalt content (AC) layer, base course, aggregate base, and subgrade (SG), from top to bottom. The inverted pavement section contained an AC layer, unbound aggregate base, cement-treated base (CTB), and subgrade. The thickness of each layer of both pavement sections was

measured and compared among the design criteria and field coring results, and a different percentage was listed in the following sections.

In this study, the objective of employing Ground Penetrating Radar (GPR) is to align the results obtained from field coring, thereby ensuring the accuracy of back-calculation for the mechanical property of each layer. The conventional method for measuring thickness via GPR utilizes the following equation:

$$h_{AC} = \frac{c \cdot t_{AC}}{2\sqrt{\varepsilon_{AC}}} \tag{1}$$

where c is the speed of light in vacuum, t_{AC} is the time difference between reflected pulses at medium interfaces and ε_{AC} is the dielectric constant of the AC layer. The value of ε_{AC} can be obtained from the Dielectric Constant Table or estimated based on literature (Plati et al., 2020; Maser and Scullion, 1992).

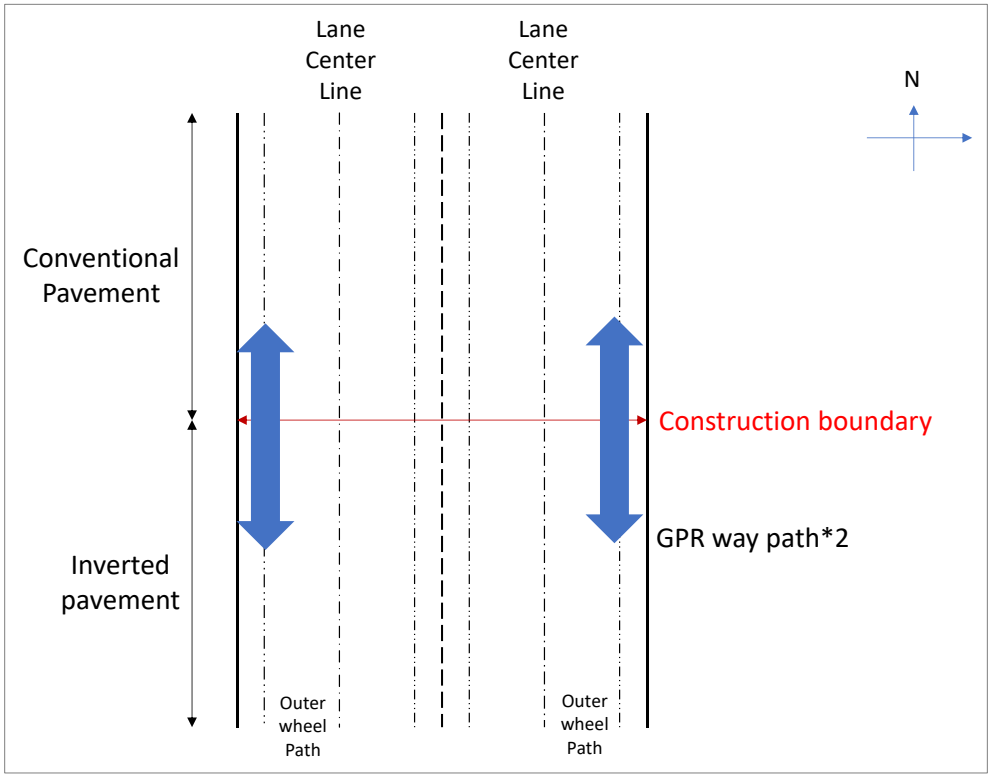

Figure 3-2. GPR scanning patterns.

3.2 Falling Weight Deflectometer (FWD)

The Falling Weight Deflectometer (FWD) is an essential nondestructive testing device extensively applied to assess conventional flexible pavement structures. A trailer-mounted device operates by dropping a specified weight onto the pavement surface. Upon the impact of the weight, sensors placed around the drop point measure the resulting deflections of the pavement. These sensors (geophones or accelerometers) are arranged at various distances from the impact area to capture a detailed deflection basin. The material properties of

pavement layers and their ability to support loads can be "inversely" back-calculated based on the measured deflection basin. The deflection measurements also provide critical information, helping engineers determine the pavement's remaining life, the need for maintenance or rehabilitation, and the effectiveness of previous repairs. The FWD data is also integral to mechanistic-empirical pavement design, where it aids in understanding the response of pavement structures to service loading conditions. It is worth noting that the accuracy of back-calculation methods in pavement analysis primarily depends on accurately capturing individual layer thickness. Therefore, coring and GPR are essential to assess pavement layer thickness and precisely ensure back-calculation quality.

Deflection basin parameters (DBPs) obtained from the FWD measurement characterize the basin shape, which can assess the structural condition of in-service pavements. DBP system originated in South Africa (Maser and Scullion, 1992; Yusoff et al., 2015) and developed in the USA. The research team adopted similar definitions and evaluation criteria to those used by Jiang et al. (2022) for assessing conventional and inverted pavement sections. Parameter SCI/BLI represents the difference of deflections measured with load geophones located at the center of the loading plate (D_0) and 300 mm (12 inches) from the center. Parameter BDI/MLI represents the difference of the deflections located at 300 mm (12 inches) and 600 mm (24 inches). Parameter BCI/LLI represents the difference of the deflections located at 600 mm (24 inches) and 900 mm (36 inches). W7 indicates the deflection at FWD's 7th sensor (1500 mm or 60 inches). Figure 3-4 shows the schematic of the FWD deflection basin curve.

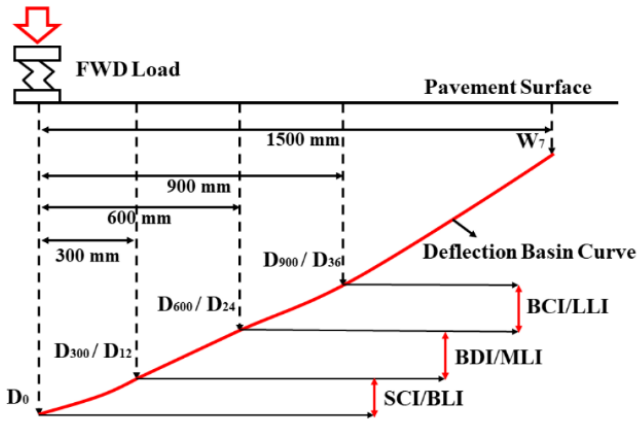

Figure 3-3. Schematic of FWD deflection basin curve.

The research team conducted two FWD measurements throughout the construction and in-use procedures of the test section in Chattanooga. The first measurement was implemented on March 24th, 2022, before paving the surface asphalt layer, while the second measurement was conducted on October 4th, 2023, after the whole pavement structure for conventional and inverted sections was completed.

- FWD before paving the surface asphalt layer.

Figure 3-4(a) illustrates the layout for FWD testing conducted before applying the surface asphalt layer. The testing pattern encompasses 27 points, with 5 points allocated to the conventional pavement section, specifically points #101, #102, #125, #126, and #127. In contrast, the inverted pavement section is more extensively tested with 22 points, ranging from

#103 to #124, systematically placed between the northern and the southern construction boundaries. The arrangement ensures a consistent spacing of 15 meters (50 feet) between each adjacent test point. Further details on the parameters and testing setup are thoroughly discussed in the subsequent discussion section.

- FWD after paving the surface asphalt layer.

Figure 3-4(b) depicts the FWD test scheme after the completion of both pavement structures. The measurements include 26 points within the inverted pavement sections, labeled #1 to #26, and 21 points within the conventional pavement sections, labeled #27 to #48. The spacing between each test point is maintained at 30.48 meters (100 feet). Notably, the arrangement of test points in the conventional sections is not symmetric due to the lane merging at the end of the north side of the conventional sections. To facilitate clarity and ease of interpretation, the test paths are named with directions and then tested accordingly: points #1 to #13 are referred to as 'inverted_southbound', points #14 to #26 as 'inverted_northbound', points #27 to #36 as 'conventional_northbound', and points #37 to #48 as 'conventional_southbound'. The second run of FWD tests was conducted using the Dynatest Fast Falling Weight Deflectometer (FFWD) provided by S&ME Inc., which is further detailed in Figure 3-5.

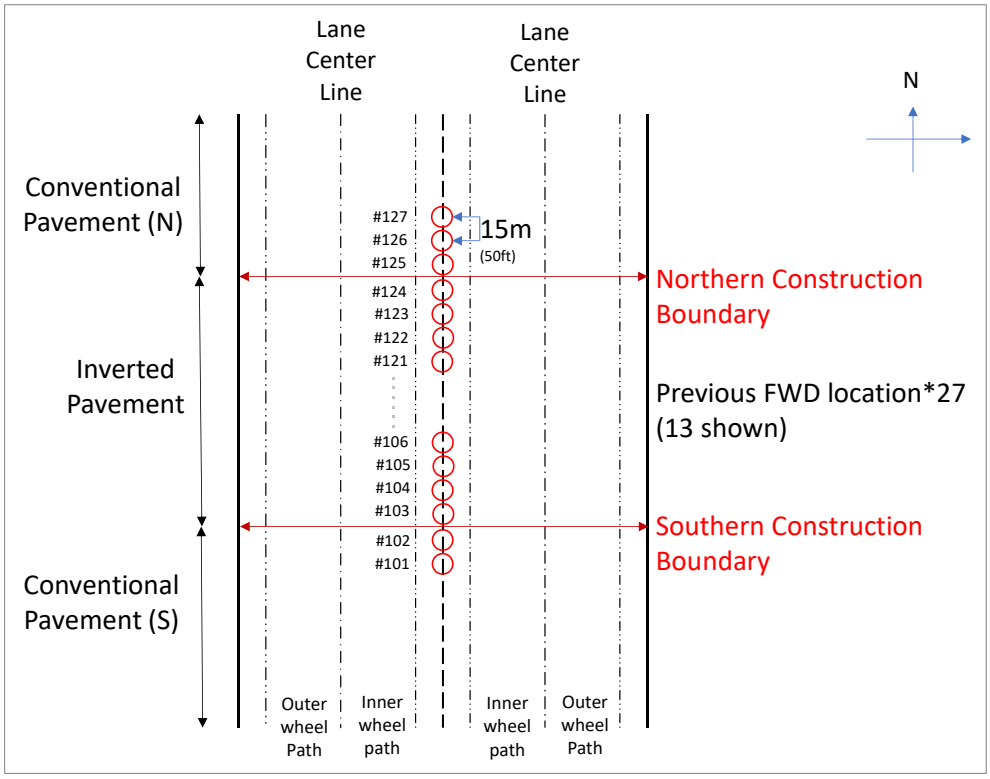

(a)

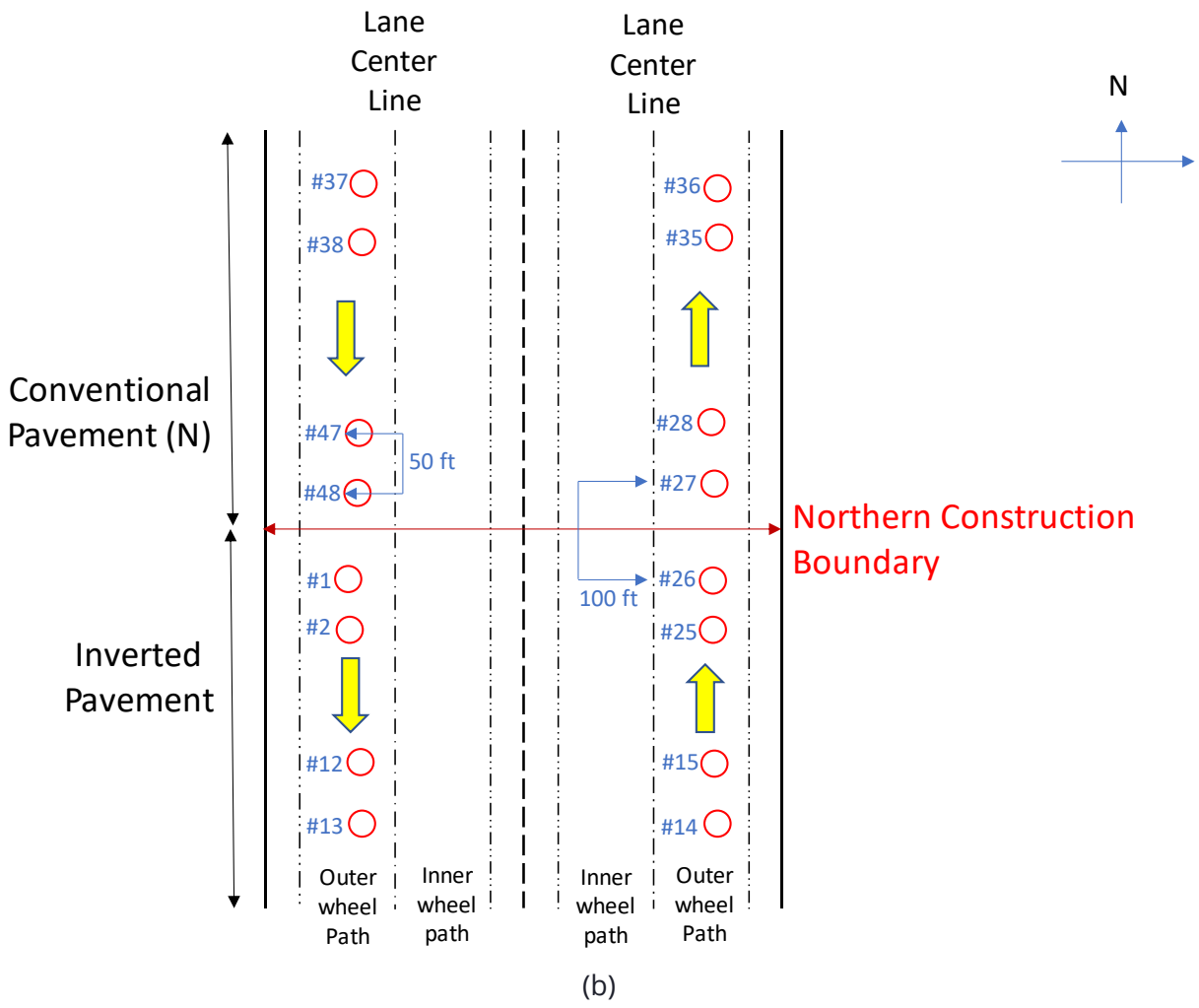

Figure 3-4. FWD test schemes: (a) before and (b) after paving surface asphalt layer for Chattanooga test pavement sections.

Figure 3-5. Fast Falling Weight Deflectometer (FFWD) setup.

3.3 Field Coring

The research team selected 8 locations near the construction boundary between conventional and inverted pavement sections. The final test locations were discussed and confirmed with TDOT. Core samples were 4 inches in diameter, sorted by depth, and labeled according to the coring locations. Long segments were cut into shorter segments to keep their height under 2 inches (50 mm). All coring locations were shown in Figure 3-6.

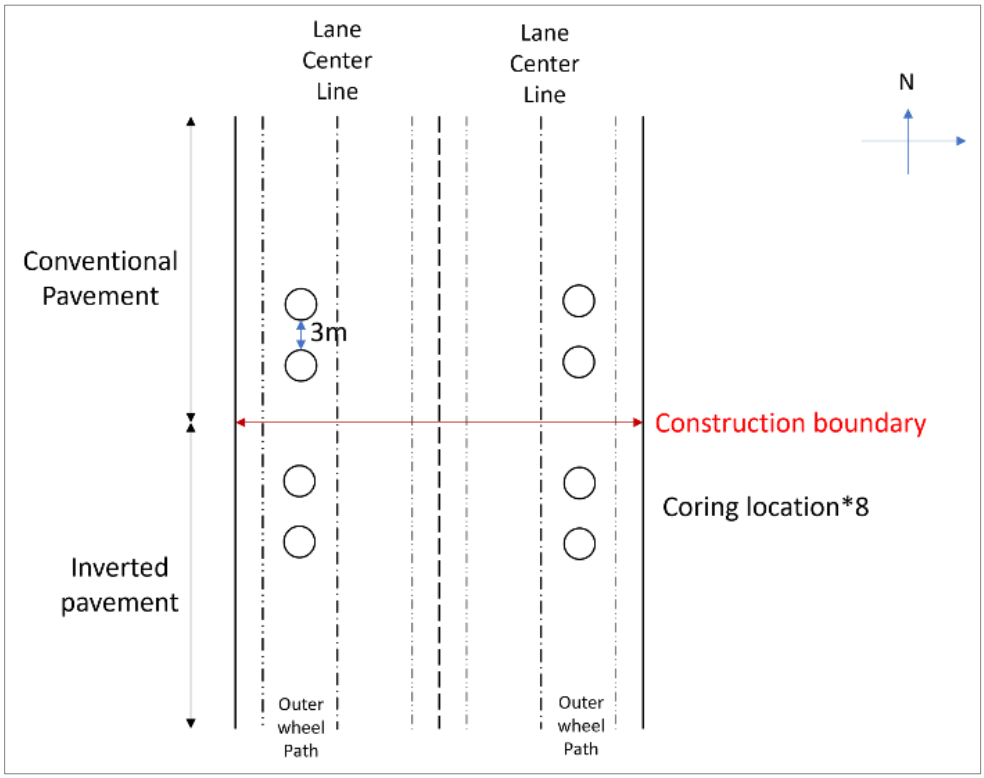

Figure 3-6. Field coring patterns.

3.4 Laboratory Resilient Modulus

The resilient modulus (MR) laboratory test is an essential procedure primarily used to assess the elastic response of pavement materials under dynamic loading conditions. It typically measures the stiffness of pavement materials, such as subgrade, subbase, base, and asphalt layers, in response to traffic-induced stresses. This test characterizes the material's ability to recover its shape after being deformed by a load, a property vital for evaluating pavement durability and performance. It measures the material's modulus of elasticity under repeated loading, simulating the conditions encountered in service traffic scenarios. The resilient modulus is particularly significant because it reflects the material's capacity to support loads over time without permanent deformation.

Figure 3-7. IDT Resilient modulus test setup.

The research team adopts the indirect tensile test (IDT) method as a viable alternative to conventional triaxial tests for conducting performance tests for resilient modulus. Witczak et al. (2002) validate the IDT method's efficacy through detailed research. An experimental setup for resilient modulus (MR) testing was developed based on the IDT criteria and procedures outlined in ASTM D7369. This setup is depicted in Figure 3-7. In this setup, four sensor handles were glued to the flat surfaces of the test specimen, each with a gauge length of 25mm. To measure applied loads and resultant deformations, Linear Variable Differential Transformers (LVDTs) were installed both horizontally and vertically, and appropriately labeled. To ensure consistency in the testing environment, the temperature was maintained at room level and controlled by a closed-door air conditioning system. The testing procedures involved applying a seating load of 50 lbf to the samples, followed by a modified sine load for a duration of 0.1 seconds and an unloading phase lasting 0.9 seconds. This cycle was repeated 30 times for each test sequence. The total resilient modulus was determined by employing the ASTM D7369 formula and the equation Witczak et al. (2002) provided for calculating Poisson's ratio.

$$M_R = \frac{P_{cyclic}}{\delta_h t}(I_1 - I_2\mu) \tag{2}$$

where M_R is the instantaneous or total resilient modulus of elasticity in MPa (psi), P_{cyclic} equals to $P_{\max} - P_{contact}$ that is the cyclic load applied to the specimen, $P_{\max}$ is maximum applied load and $P_{contact}$ is contact load in N (lb), t is the thickness of the specimen, mm (in), δ_h is recoverable horizontal (instantaneous or total) deformation in mm (in), μ is instantaneous or total Poisson's ratio (Witczak et al., 2002),

$$\mu = 0.15 + \frac{0.35}{1 + \exp(3.1849 - 0.042333 \times \text{temp})} \quad (3)$$

Since the fraction between the gauge length and the specimen diameter is close to 1/4, the constant I_1 and I_2 were selected according to ASTM D7369 recommendation. The results of the M_R for both inverted and conventional sections are shown in the discussion section.

3.5 Cost Analysis Using Pavement ME Design Software

Inverted pavement reverses the traditional layering of road materials, placing higher quality, durable materials at the bottom and less expensive materials on top. This innovative approach potentially offers several benefits. Firstly, it may save significant costs in the long term due to reduced maintenance and repair needs. The durable underneath layers are less susceptible to damage from environmental factors and heavy traffic, extending the roadway's lifespan. Secondly, using less expensive materials on the surface could reduce initial construction costs. This aspect is particularly advantageous for budget-constrained projects or regions with scarce or expensive road materials. Meanwhile, less use of natural resources like aggregates would result in less air pollution.

To validate the maintained cost benefit of inverted pavement, the research team used AASHTOWare Pavement ME Design for the preliminary cost analysis based on the laboratory and field data. Since the ME software does not include the design type and settings specifically for the inverted pavement layout, the research team used an equivalent layer to represent both the CTB layer and the subgrade. This method allows the inverted pavement structure to be simulated within the software like traditional flexible pavement with a relatively stiffer equivalent subgrade since it equivalently combines the CTB layer and subgrade together. This integrated layer is considered semi-infinite and is assigned a Poisson's ratio of 0.35. Additionally, its equivalent resilient modulus is back-calculated using FWD data via the BAKFAA software. The inputs are summarized in Figure 3-8 in the form of the Pavement ME report for both conventional and inverted sections. Regarding operational conditions, the analysis maintained the default settings for traffic data to ensure consistency. Meanwhile, the climate data was meticulously sourced from the Pavement ME website to ensure the model reflects realistic environmental conditions.

To further compare the cost-effectiveness of each pavement type, the research employs the Estimated Uniform Annual Cost (EUAC) formula:

$$EUAC = \text{cost} \times \frac{i(1+i)^n}{(1+i)^n - 1} \quad (4)$$

where *i* is discount rate (%), and *n* = service life (year). This approach, recommended by the FHWA, allows for comparing projects with different lifespans by normalizing their costs into an equivalent annual figure. Utilizing a discount rate of 4%, the analysis drew on recent local data for material costs, including prices per lane mile per inch thickness for asphalt concrete (AC), aggregate base layer, and CTB.

Design Inputs (Conventional sections)

Design Life: 20 years
Design Type: FLEXIBLE

Base construction: June, 2021
Pavement construction: September, 2021
Traffic opening: January, 2022

Climate Data Sources (Lat/Lon): 35, -85

Design Structure

Layer type	Material Type	Thickness (in)
Flexible	Default asphalt concrete	9.3
NonStabilized	Permeable aggregate	10.0
Subgrade	A-4	Semi-infinite

Volumetric at Construction:	
Effective binder content (%)	11.6
Air voids (%)	7.0

Traffic

Age (year)	Heavy Trucks (cumulative)
2022 (initial)	4,000
2032 (10 years)	3,316,470
2042 (20 years)	7,509,540

Design Inputs (Inverted section)

Design Life: 20 years
Design Type: FLEXIBLE

Base construction: June, 2021
Pavement construction: September, 2021
Traffic opening: January, 2022

Climate Data Sources (Lat/Lon): 35, -85

Design Structure

Layer type	Material Type	Thickness (in)
Flexible	Default asphalt concrete	2.3
NonStabilized	Permeable aggregate	15.0
Subgrade	A-4	Semi-infinite

Volumetric at Construction:	
Effective binder content (%)	11.6
Air voids (%)	7.0

Traffic

Age (year)	Heavy Trucks (cumulative)
2022 (initial)	4,000
2032 (10 years)	3,316,470
2042 (20 years)	7,509,540

Figure 3-8. Example of Pavement ME inputs for conventional and inverted sections.

Chapter 4 Results and Discussion

4.1 Field investigation location

The test pavement site is located at 7531-7543 Ferdinand Piech Way, Chattanooga, TN, featuring a configuration of four lanes in each direction with an additional center left-turn lane, as illustrated in Figure 4-1. The total test sections are 0.3 miles, including 0.2 miles of conventional pavement and 0.1 miles of inverted pavement. To evaluate these sections, a series of tests were employed, including the Falling Weight Deflectometer (FWD), Ground Penetration Radar (GPR), pavement coring, and pavement profiling, conducted within the parameters set by TDOT for traffic control, specifically between lane centerlines and the outer wheel paths. Figure 4-2 shows the designed profile of the conventional and the inverted pavement sections. Notably, the inverted pavement section comprises two thin asphalt layers with a total thickness of 57.15 mm, an aggregate base of grading D, and a cement-treated base (CTB) layer atop the subgrade. The conventional section has much thicker asphalt layers with a total thickness of 234.95 mm and doesn't have a CTB layer.

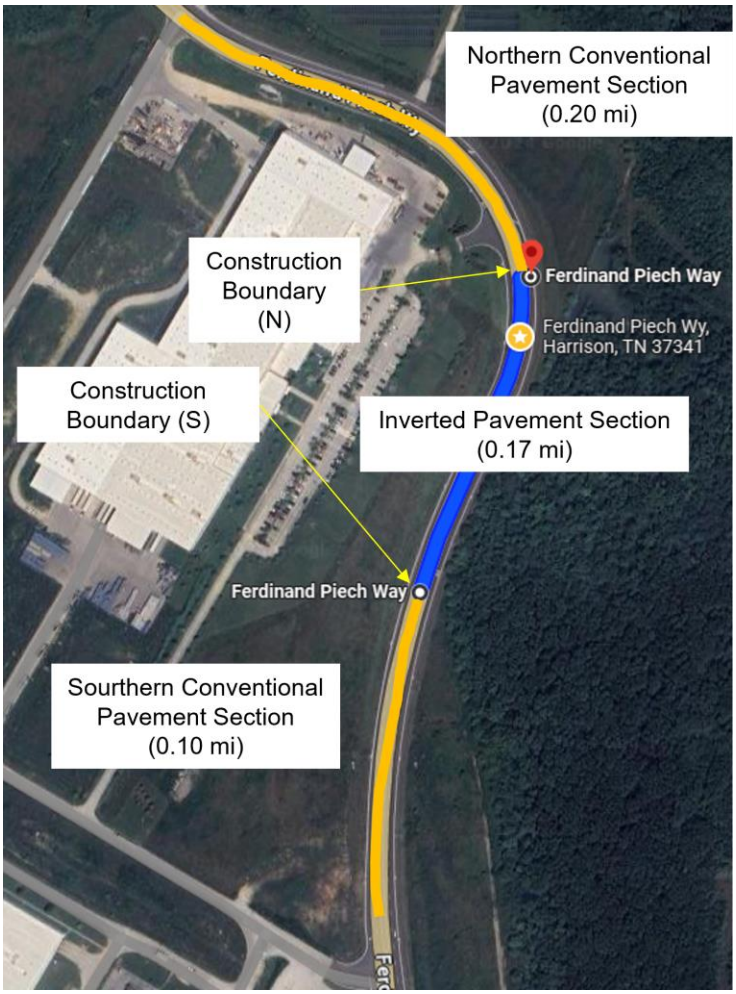

Figure 4-1. The conventional and inverted pavement test sections in Chattanooga, TN.

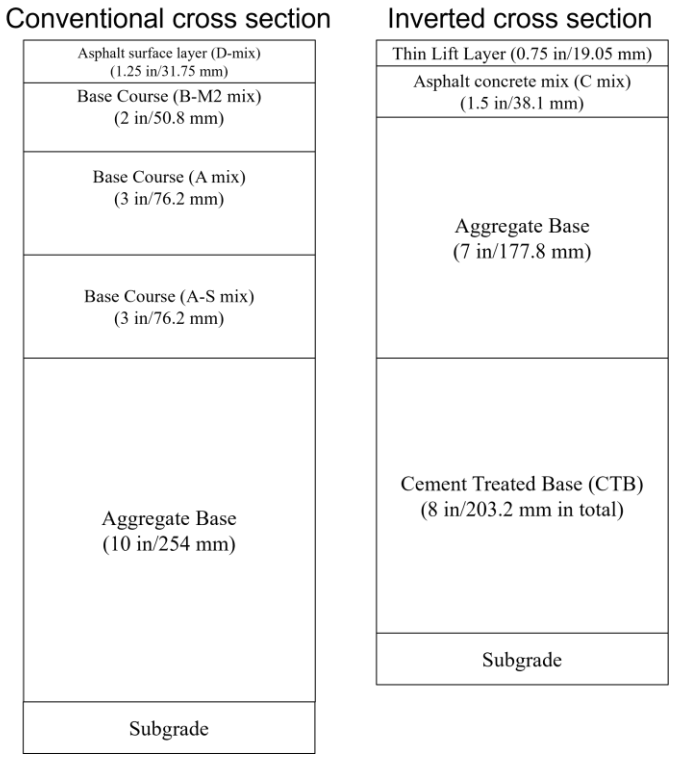

Figure 4-2. The conventional and inverted pavement test sections in Chattanooga, TN.

4.2 GPR results

The conventional and inverted sections are constructed according to the designed profile detailed in Figure 4-2. The thickness of each layer of both configurations was measured and verified using GPR. The images were further analyzed to achieve the whole pavement layer information. Figure 4-3 depicts a cross-sectional view of pavement structures, comparing conventional pavement on the left to inverted pavement on the right, as indicated by the labels. Both sections are delineated by vertical red dashed lines, highlighting the differences in layer composition. Different color bands in the GPR scanning image denote each subsurface layer with various materials. Therefore, the thickness of each layer can be visually identified and illustrated by the yellow dashed lines. Two different pavement structures are clearly observed in the image, and the thickness of their structure sublayers is given in Table 4-1. The GPR measurement will be evaluated with field coring results, the detailed comparison lies in Section 4.3.

Table 4-1. GPR SCANNED LAYER THICKNESS OF TESTING PAVEMENTS.

Conventional section		*Inverted section*	
Structure layer	Thickness	Structure layer	Thickness
Asphalt Concrete	1.52 in (38.61 mm)	Asphalt Concrete	2.96 in (75.18 mm)
Based Course	7.87 in (199.90 mm)	Aggregate Base	7.87 in (199.90 mm)
Aggregate base	10 in (254 mm)	Cement Treated Base	9.84 in (249.94 mm)
Subgrade	-	Subgrade	-

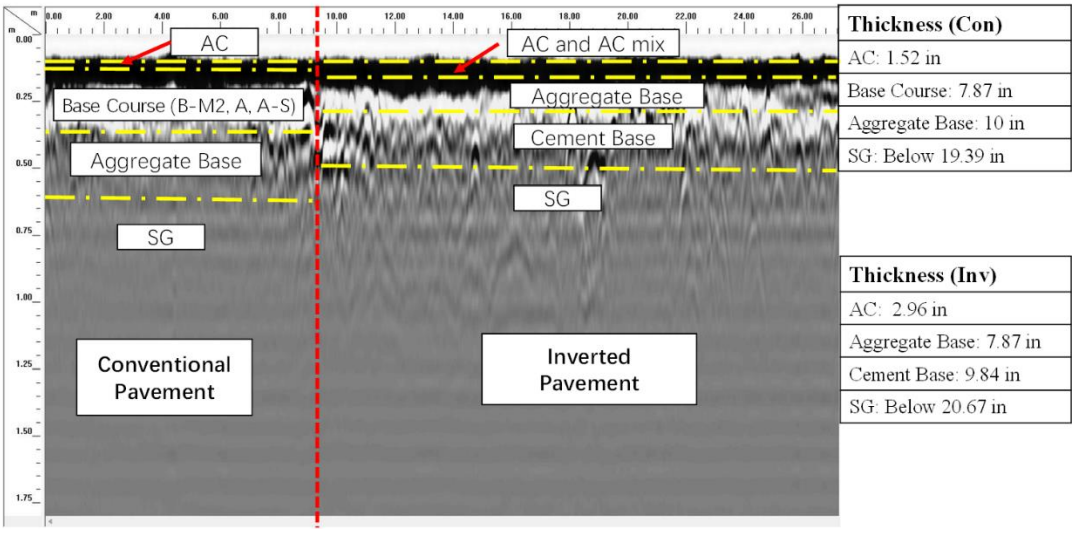

Figure 4-3. Result of GPR measurement of pavement layer thickness.

4.3 Field coring results

Accurately measuring the thickness of structural layers in both conventional and inverted pavement sections is critical for predicting service life and conducting cost/benefit analysis with Pavement ME Design software. Therefore, the research team cored four samples each for both pavement sections to compare with the designed thicknesses and GPR scanning. The thicknesses of layered cores are measured and sorted from top to bottom by coring sections. Firstly, the designed thickness is summarized according to the TDOT CAD drawing (CNU221-Typical section) in **Error! Not a valid bookmark self-reference.** and Table 4-3.

Table 4-2. INVERTED PAVEMENT LAYER THICKNESS REFERENCE (TODT, CNU221).

Design #	*Layer type*	*Design thickness*
20	Thin Lift layer	0.75
16	Asphalt Concrete mix (C mix)	1.5
15	Aggregate base	7
17	Aggregate cement base course	8

Table 4-3. CONVENTIONAL PAVEMENT LAYER THICKNESS REFERENCE (TODT, CNU221).

Design #	*Layer type*	*Design thickness*
8	Asphalt surface layer (D-mix)	1.25
3	Binder course (BM2 mix)	2
13	Base course (A-mix)	3
14	Base course (A-S mix)	3
1	Aggregate base	10

Table 4-4 shows the layer thickness of inverted pavement measured from the extracted cores. The thickness of the thin lift layer for core samples is slightly higher than the design value, while the thickness of the C mix layer presents a similar value to the design thickness. The aggregate base layer was crushed into pieces during coring, while the cement-treated base (CTB) layer for all cored samples was incomplete due to the limited depth during coring. Hence, the

thicknesses of these layers are not available for cores but can be evaluated through GPR scanning. Table 4-5 shows the layer thickness of the conventional pavement measured from the extracted cores. All conventional cores were more complete than those extracted from inverted sections, presenting a more accurate layer thickness estimation. The thicknesses of all conventional pavement layers closely match the designed specifications, signifying high construction quality.

A general comparison between the TDOT design criteria (CNU221) and field GPR results is summarized in Table 4-6. For the inverted section, the coring difference is larger than the GPR difference based on the coring process and the layer material properties. It can be found that the aggregate base layer also presents a similar thickness as the designed value.

Table 4-4. INVERTED SECTION CORES SUMMARY.

Design #	*Layer type*	*Design thickness (in)*	*Core thickness (in)*	*Difference %*
Western Core 1	Thin Lift layer	0.75	1.54	105.33%
	C mix	1.5	2.05	36.67%
	Aggregate base	7	N/A	N/A
	Aggregate cement base course	8	N/A	N/A
Western Core 2	Thin Lift layer	0.75	1.55	106.67%
	C mix	1.5	1.83	22.00%
	Aggregate base	7	N/A	N/A
	Aggregate cement base course	8	N/A	N/A
Eastern Core 1	Thin Lift layer	0.75	1.54	105.33%
	C mix	1.5	1.95	30.00%
	Aggregate base	7	N/A	N/A
	Aggregate cement base course	8	N/A	N/A
Eastern Core 2	Thin Lift layer	0.75	1.55	106.67%
	C mix	1.5	1.54	2.67%
	Aggregate base	7	N/A	N/A
	Aggregate cement base course	8	N/A	N/A

Table 4-5. CONVENTIONAL SECTION CORES SUMMARY.

Design #	*Layer type*	*Design thickness (in)*	*Core thickness (in)*	*Difference %*
Western Core 1	Asphalt surface layer (D-mix)	1.25	1.57	25.60%
	Binder course (BM2 mix)	2	2.23	11.50%
	Base course (A-mix)	3	3.02	0.67%
	Base course (A-S mix)	3	3.20	6.67%
	Aggregate base	10	N/A	N/A
Western Core 2	Asphalt surface layer (D-mix)	1.25	1.38	10.40%
	Binder course (BM2 mix)	2	2.64	32.00%
	Base course (A-mix)	3	2.91	3.00%
	Base course (A-S mix)	3	3.17	5.67%
	Aggregate base	10	3.35	66.50%
Eastern Core 1	Asphalt surface layer (D-mix)	1.25	1.57	25.60%
	Binder course (BM2 mix)	2	2.28	14.00%
	Base course (A-mix)	3	3.07	2.33%
	Base course (A-S mix)	3	2.96	1.33%

	Aggregate base	10	N/A	N/A
Eastern Core 2	Asphalt surface layer (D-mix)	1.25	1.85	48.00%
	Binder course (BM2 mix)	2	1.97	1.50%
	Base course (A-mix)	3	3.34	11.33%
	Base course (A-S mix)	3	3.15	5.00%
	Aggregate base	10	N/A	N/A

Table 4-6. GPR AND FIELD CORING COMPARISON.

	Inverted			*Convention*		
	Asphalt layer	*Aggregate base*	*Cement base course*	*Asphalt layer*	*Base course*	*Aggregate base*
Design (in)	2.25	7.00	8.00	1.25	8.00	10.00
Field GPR (in)	2.96	7.87	9.84	1.52	7.87	10.00

4.5 Laboratory Resilient Modulus results

The research team conducted a series of resilient modulus tests on the cored specimens to assess the elastic response of materials for the structure layers of conventional and inverted pavements under dynamic loading conditions. The labeled test specimens are shown in Figure 4-4. Since the condition of cored samples was not ideal, the inverted section specimen lost most of the CTB layers and aggregate base layers, leading to fewer test specimens than the conventional sections. According to the recommendation in ASTM D7369, the constant I_1 is 0.144357, and I_2 is -0.450802. The MR testing procedure recorded 1024 data points per second for 0.1s load duration by the MTS system. Both specimens from conventional and inverted sections were applied to the same load cycles. The resilient modulus of tested samples is determined using the averaged value of the resilient modulus measured during the last five cycles, which are summarized in Table 4.7 and 4-8.

The tested resilient modulus is utilized as the initial trial value in back-calculation. Therefore, the absent layer properties can be obtained using FWD back-calculation. Since the aggregate layers of inverted sections are not complete after coring, the research team used 30 ksi as the origin modulus of the aggregate base (Papadopoulos and Santamarina, 2019), which was modeled by LTPP Material Code 303 Crushed Stone (Jiang et al., 2022). The instantaneous deformation lies in the transition zone between the unloading path and recovery portion, and the total deformation lies in the 85% to 95% rest period. According to equation (2), the value of resilient modulus only depends on the recoverable horizontal deformation since other parameters are constant. The research team used instantaneous and total deformation for comparison during resilient modulus calculation.

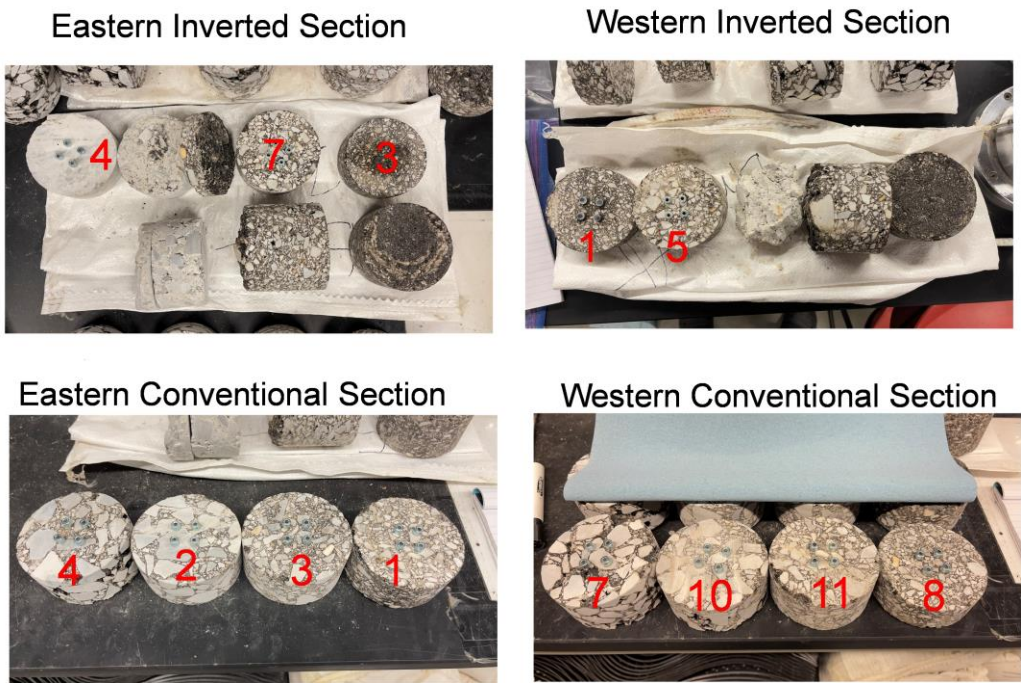

Figure 4-4. Labeled Resilient Modulus samples, categorized by pavement sections.

Table 4-7. AVERAGED RESILIENT MODULUS VALUES OF INVERTED SECTIONS.

Specimen #	*Layer type*	*Averaged calculated MR (psi)*
East Inv. 3	Thin lift layer	102,732
East Inv. 4	Cement treated base	1,457,048
East Inv. 7	Thin lift layer	195,591
West Inv. 1	Thin lift layer	214,501
West Inv. 5	Thin lift layer	126,687

Table 4-8. AVERAGED RESILIENT MODULUS VALUES OF CONVENTIONAL SECTIONS.

Specimen #	*Layer type*	*Averaged calculated MR (psi)*	*Notes*
East Con 1	Asphalt surface layer (D mix)	184,214	
East Con. 2	Base course (A-mix)	613212	
East Con. 3	Binder course (BM2 mix)	676381	
East Con. 4	Base course (A-S mix)	N/A*	Broken sample
West Con. 7	Base course (A-S mix)	133991	
West Con. 8	Asphalt surface layer (D mix)	151622	
West Con. 10	Base course (A-mix)	629035	
West Con. 11	Base course (BM2 mix)	1392551	

4.6 Back-Calculation of FWD Test Before Paving Surface Layer

4.6.1 FWD back-calculation before Paving Surface Layer

The research team analyzes the results of FWD data using back-calculation methods to obtain pavement layer moduli, pavement structural number, subgrade soil modulus, and pavement surface deflection. The software used by the research team is BAKFAA v3.4. The BAKFAA

software is the Federal Aviation Administration's (FAA) specialized software designed for back-calculating pavement material properties by analyzing data from Heavy Weight Deflectometer/Falling Weight Deflectometer (HWD/FWD) tests. The user can select given pavement-type templates or customized ones for each layer. The parameters of materials are collected from other verified literature (Papadopoulos and Santamarina, 2015; Khan and Nagabhushana, 2020; Jiang et al., 2022) and listed in Table 4-9. The back-calculation parameters of both conventional and inverted sections are shown in Table 4-10. All FWD data were input into BAKFAA software for back calculations, including five locations in the conventional section (points 101, 102, 125, 126, 127) and 22 locations in the inverted section (points 103 to 124). Since the FWD was conducted before surface layer paving, the back calculations did not include asphalt content layers in both conventional and inverted sections.

Table 4-11 summarizes the modulus of the structure layers from FWD back-calculation and resilient modulus tests. Certain parts of the comparison between the back-calculation results and resilient modulus are missing due to constraints in the available data. Based on the data shown in Table 4-11, it indicates that the calculated resilient modulus values fall within the recommended range specified in the BAKFAA manual despite being lower than the typical value. During the back-calculation process, the binder and base courses of the conventional sections were treated as a single layer and employed a higher initial guess of its modulus. Since the top layer was not laid down when the first FWD measurement was conducted, the layers' modulus from the first FWD back-calculation may not accurately represent the completed structure.

Table 4-9. TYPICAL MODULUS VALUES AND RANGE FOR PAVING MATERIALS (BAKFAA V3.4 MANUAL)

Material	*Item number*	*Low value*		*Typical value*		*High value*	
		psi	MPa	psi	MPa	psi	MPa
Asphalt Mix Pavement	P-401/P-403	70,000	500	500,000	3,500	2,000,000	14,000
Cement concrete pavement	P-501	1,000,000	7,000	5,000,000	35,000	9,000,000	60,000
Lean concrete base course	P-306	1,000,000	7,000	2,000,000	14,000	3,000,000	20,000
Asphalt treated base	P-304	100,000	700	500,000	3,500	1,500,000	10,000
Cement treated base		200,000	1,400	750,000	5,000	2,000,000	14,000
Aggregate base course	P-208/P-209	10,000	70	30,000	200	50,000	350
Granular subbase course	P-154	5,000	30	15,000	100	30,000	200
Stabilized soil		10,000	70	50,000	350	200,000	1,400
Cohesive soil		3,000	20	7,000	50	25,000	170

Table 4-10. FWD PARAMETERS IN BACK CALCULATIONS

Layer (Conventional)	*Seed Modulus (psi)*	*Poisson's ratio*	*Interface Parameter*	*Thickness (in)*
Asphalt layer	500,000	0.35	1.00	1.25
Bases course (B-M2, A, A-S)	1,500,000	0.35	1.00	8
Aggregate base	50,000	0.35	1.00	10
Subgrade	30,000	0.4	1.00	∞
Layer (Inverted)	*Seed Modulus (psi)*	*Poisson's ratio*	*Interface Parameter*	*Thickness (in)*
Asphalt layer	500,000	0.35	1.00	2.25
Aggregate base	200,000	0.35	1.00	7

Cement base course	2,000,000	0.2	1.00	8
Subgrade	50,000	0.4	1.00	∞

Table 4-11. SUMMARY OF BACK-CALCULATED MODULUS AND MR TESTING RESULTS.

Core Section	*Layer*	*Back-calculated modulus (psi)*	*M_R field (psi)*
Western Inverted Section	Thin Lift layer	N/A	193,946
	BM2 mix	N/A	263,773
	Aggregate base	170,467	N/A
	Cement treated base	1,635,979	N/A
Eastern Inverted Section	Thin Lift layer	N/A	159,134
	BM2 mix	N/A	301,577
	Aggregate base	170,467	N/A
	Cement treated base	1,635,979	N/A
Western Conventional Section	Asphalt surface layer (D-mix)	N/A	248,579
	Binder course (BM2 mix)	964,497 combined	283,217
	Base course (A-mix)		266,805
	Base course (A-S mix)		212,057
	Aggregate base	294,077	N/A
Eastern Conventional Section	Asphalt surface layer (D-mix)	N/A	238,818
	Binder course (BM2 mix)	964,497 combined	276,663
	Base course (A-mix)		299,569
	Base course (A-S mix)		202,023
	Aggregate base	294,077	N/A

4.6.2 FWD back-calculation after Paving Surface Layer (FFWD)

The same back-calculation software, BAKFAA version 3.4, was utilized for determining the modulus of pavement layers for both conventional and inverted sections upon completion of the entire structure. The parameters used for the back-calculation in both section types are detailed in Table 4-12. The modulus values derived from the back-calculation, based on data collected by the first Falling Weight Deflectometer (FWD) before the paving of the surface layer, indicated challenges in fine-tuning the process. As a result, these back-calculated modulus values may not be suitable for further analysis. The back-calculated results from the second FWD measurements are summarized in Table 4.13.

Table 4-14 integrates the resilient modulus tested from coring samples and the back-calculated modulus. The percent difference is divided by the resilient modulus value from coring. It is concluded that the back-calculated modulus is generously greater than the MR value from coring, which may be due to the back-calc mechanism and the layer definitions. The modulus of the treated base is estimated due to the lack of successfully cored samples. Since the in-situ coring for both conventional and inverted sections is not fully penetrated to the subgrade layers, further studies may require better sample coring methods and better MR back-calc tuning of the parameters.

Table 4-12. FWD PARAMETERS IN BACK CALCULATIONS (FFWD).

Layer (Conventional)	*Seed Modulus (psi)*	*Poisson's ratio*	*Interface Parameter*	*Thickness (in)*
Asphalt layer	167,917	0.35	1.00	1.25
Bases course (B-M2)	1,034,466	0.35	1.00	2.00

Base course (A)	621,123	0.35	1.00	3.00
Base course (A-S)	133,990	0.35	1.00	3.00
Aggregate base	29,366	0.35	1.00	10.00
Subgrade	20,961	0.4	1.00	∞
Layer (Inverted)	*Seed Modulus (psi)*	*Poisson's ratio*	*Interface Parameter*	*Thickness (in)*
Thin lift layer	157,133	0.35	1.00	0.75
C mix	774,286	0.35	1.00	1.50
Aggregate base	29,366	0.35	1.00	7.00
Cement base course	1,457,048	0.2	1.00	8.00
Subgrade	20,961	0.4	1.00	∞

Table 4-13. BACK-CALCULATED MODULUS OF STRUCTURE LAYERS.

M_R (Inverted)			*M_R (Conventional)*		
Layer	*Inverted_SB (psi)*	*Inverted_NB (psi)*	*Layer*	*Conventional_ SB (psi)*	*Conventional_ NB (psi)*
Thin lift layer	190345	175234	Asphalt layer	183239	193056
C mix	866021	808866	Binder course (B-M2)	1132477	1124694
Aggregate base	33247	30478	Base course (A)	712000	683124
Cement treated base	750000	750000	Base course (A-S)	154157	155778
Subgrade layer	27411	20347	Aggregate base	29366	29366
			Subgrade layer	23612	26338

Table 4-14. COMPARISON OF TESTED AND BACK-CALCULATED MR RESULTS.

Pavement type	*Layer*	*Tested M_R (psi)*	*Back-calculated M_R (psi)*	*Difference %*
Inverted	Thin lift layer	159878	182789	14.33%
	C mix	774286	837444	8.16%
	Aggregate base	N/A	31863	N/A
	Cement treated base	1457048	750000	48.53%
	Subgrade layer	20961	23879	13.92%
Conventional	Asphalt layer	167918	188147	12.05%
	Binder course (B-M2)	1034466	1128586	9.10%
	Base course (A)	621124	697562	12.31%
	Base course (A-S)	133991	154968	15.66%
	Aggregate base	N/A	29366	N/A
	Subgrade layer	20961	24975	19.15%

4.7 DBPs system analysis

The research team used the same definition and criteria for evaluating the deflection basin parameters for the FWD data from Jiang et al., 2022. For the first FWD test, although the surface layer for both conventional and inverted sections is not paved, it is still meaningful as a reference to compare the second FWD measurement and future FWD data. In this study, a 9000 lbs load was applied at 20 m intervals along the pavement. Deflections were recorded by seven sensors at radial distances of 0 in (D_0), 12 inches (D_{300}), 18 inches, 24 inches (D_{600}), 36 inches (D_{900}), 48 inches, and 60 inches (W_7) from the center of a loading plate with a 150 mm radius. The definitions of DBP parameters are shown in Figure 4-5. The DBPs derived from 2nd FFWD test are summarized in Table 4-17.

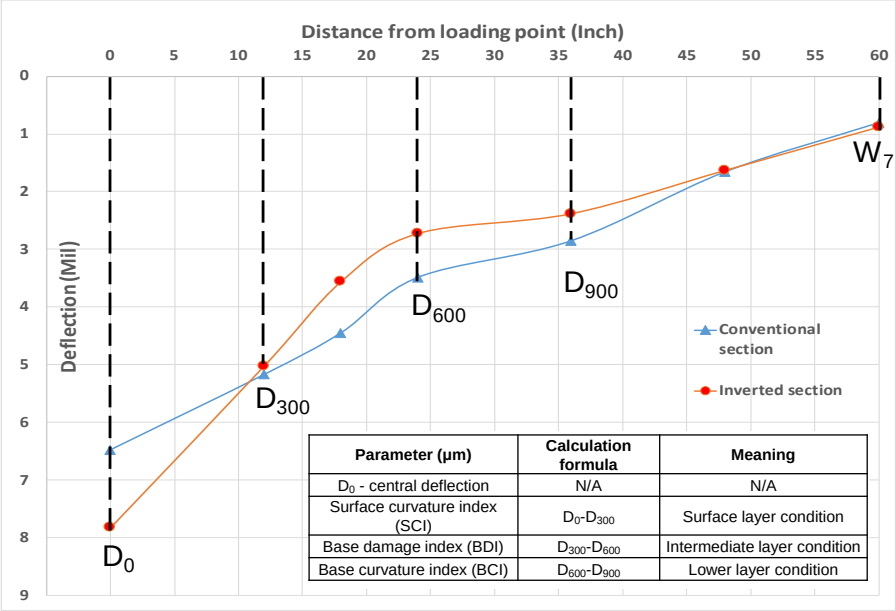

Figure 4-5. Definition and calculation of deflection basin parameters based on deflection basins of inverted and conventional pavement sections.

Horak et al. (2015) developed a comprehensive evaluation system with specific threshold values based on the Deflection Basin Parameters (DBPs) for South Africa (Table 4-15). Chang et al. (2014) introduced structural condition indices in Texas, USA, utilizing Falling Weight Deflectometer (FWD) data and layer thickness measurements to identify potential distressed layers (Table 4-16). Both systems employ the FWD testing method with a 9000 lbs load, differing primarily in their rating levels. The assessment system in South Africa categorizes condition ratings into three levels for each parameter: sound, warning, and severe. In contrast, the American system offers four condition ratings: very good, good, fair, and poor. These methodologies were initially designed for conventional pavement structures.

Table 4-15. THRESHOLD VALUES FOR 40 KN LOAD ON A GRANULAR BASE PAVEMENT (HORAK ET AL. 2015).

Evaluation Results	*D_0*	*SCI (BLI)*	*BDI (MIL)*	*BCI (LLI)*
Sound	<500	<200	<100	<50
Warning	500-750	200-400	100-200	50-100
Severe	>750	>400	>200	>100

Table 4-16. THRESHOLD VALUES FOR 40 KN LOAD ON A GRANULAR BASE PAVEMENT (CHANG ET AL. 2014).

Index Parameters	*Asphalt Thickness*		*Diagnosis*
	> 5 inch **Conventional**	>= 1 inch, < 2.5 inch **Inverted**	
SCI	< 101.6	< 304.8	Very good Asphalt layer
	101.6 - 152.4	304.8 - 457.2	Good Asphalt layer
	152.4 - 203.2	457.2 - 609.6	Fair Asphalt layer
	203.2 - 254	609.6 - 762	Poor Asphalt layer
	> 254	> 762	Very poor Asphalt layer
BCI	< 50.8	< 101.6	Very good Base layer
	50.8 - 76.2	101.6 - 203.2	Good Base layer
	76.2 - 101.6	203.2 - 304.8	Fair Base layer

	101.6 - 127	304.8 - 406.4	Poor Base layer
	> 127	> 406.4	Very poor Base layer
W7	< 25.4	< 25.4	Very good Subgrade layer
	25.4 - 35.56	25.4 - 35.56	Good Subgrade layer
	35.56 - 45.72	35.56 - 45.72	Fair Subgrade layer
	45.72 - 55.88	45.72 - 55.88	Poor Subgrade layer
	> 55.88	> 55.88	Very poor Subgrade layer

Following the DBPs-based rating criteria established by Jiang et al. (2022), the research team conducted preliminary ratings of pavement sections, as summarized in Table 4-17 and Table 4-18. The conventional and inverted pavement sections received very good and good ratings according to the established criteria. It is found that the average values of SCI in the inverted pavement are 107.52 µm for Northbound and 131.25 µm for Southbound, which are larger than the SCI values of 62.78 µm for Northbound and 58.57 µm for Southbound in the conventional pavement. The differences are due to the thickness of the asphalt layer. The AC layer of the inverted pavement has a thickness that is just one-fourth the thickness of the AC layer in the conventional pavement section. Thus, the same pulse load induced more deflection on the AC layer in the inverted pavement section. Short-term monitoring indicated that inverted and conventional structures are rated similarly based on the DBPs system. Nonetheless, long-term performance assessment requires further field testing and measurements to validate these findings.

Table 4-17. DEFLECTION BASIN PARAMETERS FOR CONVENTIONAL AND INVERTED SECTIONS.

Section #	*Average D_0 (µm)*	*Average D_{300} (µm)*	*Average D_{600} (µm)*	*SCI (µm)*	*BDI (µm)*	*BCI (µm)*	*W7 (µm)*
Conventional NB	165.13	102.35	34.85	62.78	67.5	28.95	25.1
Conventional SB	169.05	110.48	36.30	58.57	74.18	31.64	26
Inverted NB	195.39	87.87	36.07	107.52	51.81	19.46	26.92
Inverted SB	243.50	112.25	37.34	131.25	74.91	29.73	27.69

Table 4-18. DEFLECTION BASIN PARAMETERS AND STRUCTURAL CONDITION INDICES FOR DISTRESSED LAYERS.

	Inverted Section		*Conventional Section*	
	Northbound	*Southbound*	*Northbound*	*Southbound*
SCI (µm)	107.52	131.25	62.78	58.57
Rating	Very good AC layer (SCI <304.8)		Very good AC layer (SCI <150)	
BDI (µm)	-	-	67.50	74.18
Rating	-		Sound UAB layer (BDI<100)	
BCI (µm)	19.46	29.73	-	-
Rating	Very good UAB + CTB layer (BCI < 101.6)		-	
W7 (µm)	26.92	27.69	25.1	26
Rating	Good SG layer (25.4 < W7 < 35.56)		Very good (W7 < 25.4) SG layer Good (25.4 < W7 < 35.56) SG layer	

4.8 Field ride quality profiles

The terms "roughness" and "smoothness" are often used interchangeably in pavement analysis, referring to aspects beyond ride quality, such as vehicle delay costs, fuel consumption, and maintenance costs (UMTRI, 1998). The Chattanooga test pavement site, having been recently completed and opened for service, displays no signs of cracking or severe rutting.

Therefore, the research team comprehensively evaluated the roughness for both conventional and inverted pavement sections. The profiler tests of ride quality were conducted by TDOT. Specifically, the profiler tests indicated that the inverted pavement section on the southbound lane extended from 0.25 miles to 0.42 miles and on the northbound from 1.25 miles to 1.45 miles. Figure 4-6 illustrates the profiler test patterns for both pavement types across the two directions.

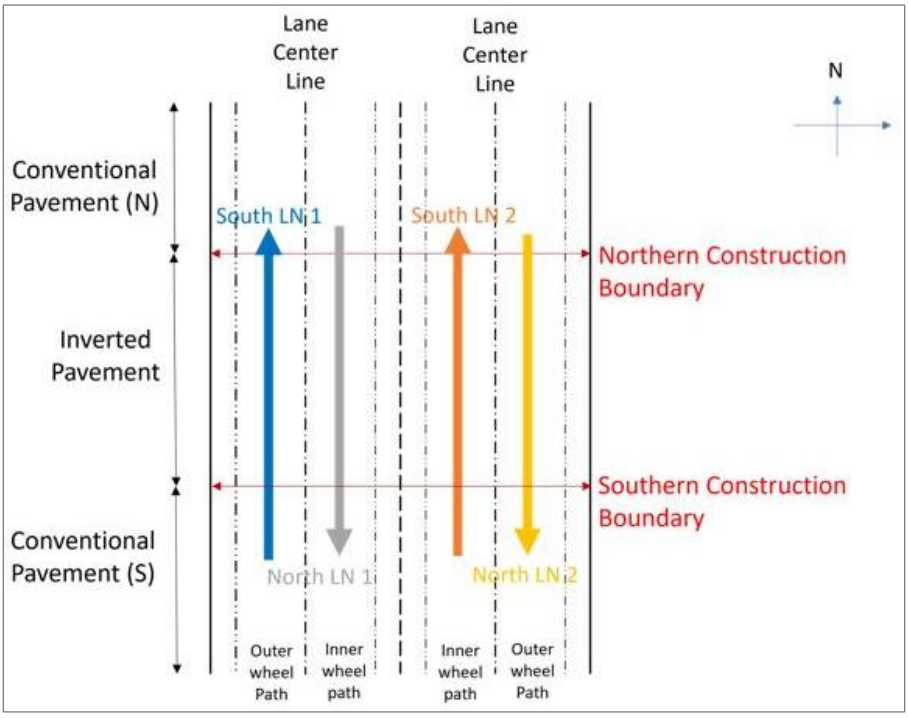

Figure 4-6. Profiler testing patterns for different pavement sections.

Figure 4-7 the continuous Mean Roughness Index (MRI) was shown across all evaluated pavement sections. The MRI, computed as the average of the International Roughness Index (IRI) values from both the left and right wheel paths, serves as a metric for assessing ride quality. To facilitate comparison across the four subfigures, yellow dashed lines indicating the same MRI level of 350 in/mi have been superimposed to delineate a consistent MRI range. The inverted pavement sections are of particular interest and are highlighted with red flags and ranged by double-headed arrows.

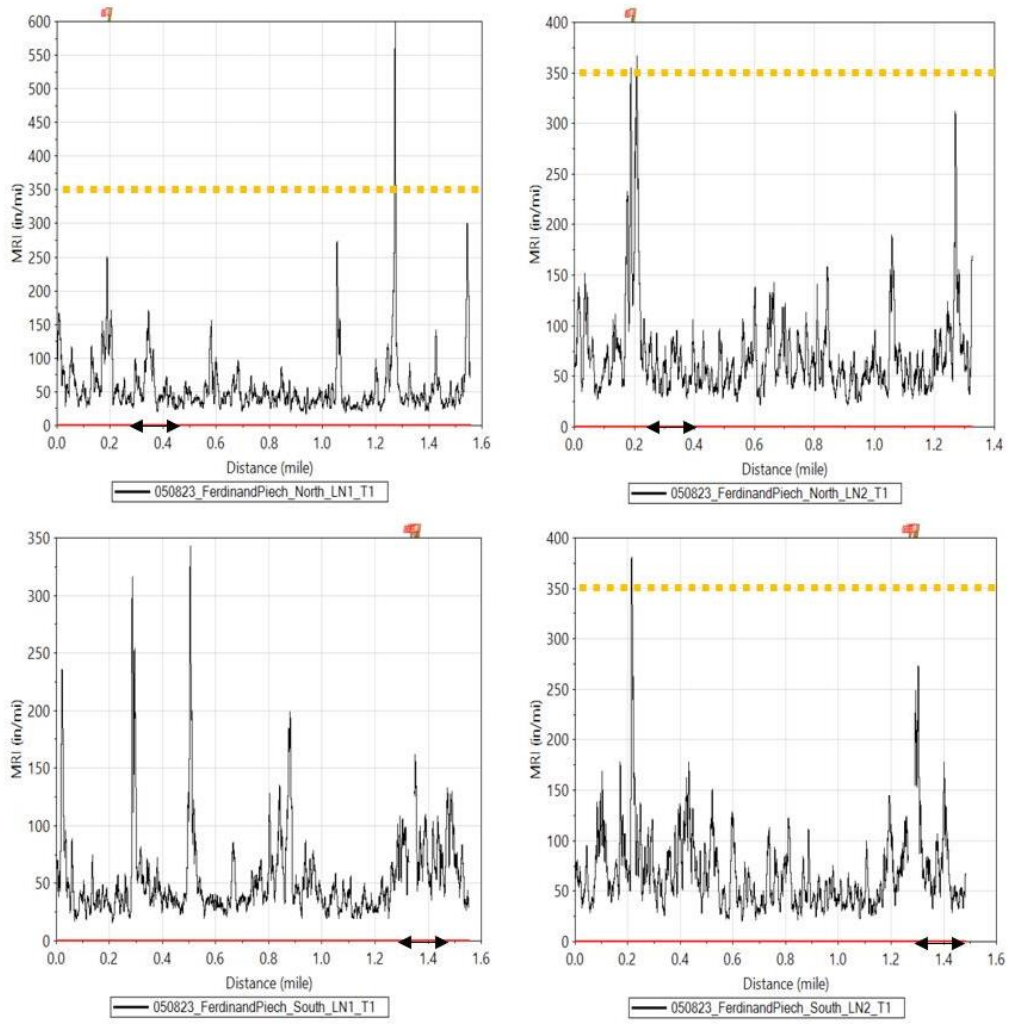

Figure 4-7. Detailed MRI results.

Table 4-19 shows federal pavement roughness thresholds for interstate facilities (FHWA, 1999). In this study, since MRI is the average value of left-wheel and right-wheel IRI, the research team summarized the MRI value and compared it to the FHWA criteria; the results and calculated difference in percentage are summarized in Table 4-20. According to Table 4-19, three tested inverted sections rate "Very Good", and only one section North LN 2 is rated as "Good". For the conventional section, the South LN 1 and North LN 2 sections rate "Good", and the rest rate" Very Good". Since the traffic loads varied from the lanes and driving directions, the difference in MRI between construction sections in one lane is smaller than in MRI between lanes. However, in the South LN 1 section, the conventional section has a larger difference than the inverted section, indicating that the inverted section can maintain roughness better than the conventional section under certain traffic loads. For other lanes, the general difference is less than 5%, which can be due to construction and measurement variations. Since a smaller IRI indicates a smoother surface and better ride quality, MRI can be a direct index for evaluating the ride quality of selected pavement sections.

Table 4-19. FEDERAL PAVEMENT ROUGHNESS THRESHOLDS FOR INTERSTATE FACILITIES (FHWA, 1999).

Condition Term	*PSR Rating*	*IRI*	*NHS Ride Quality*
Very Good	≥ 4.0	< 60 in/mi (< 0.95 m/km)	Acceptable: 0- 170
Good	3.5 – 3.9	60 – 94 in/mi (0.95 – 1.48 m/km)	
Fair	3.1 – 3.4	95 – 119 in/mi (0.95 – 1.48 m/km)	
Mediocre	2.6 – 3.0	120 – 170 in/mi (1.89 – 2.68 m/km)	
Poor	≤ 2.5	> 170 in/mi (> 2.68 m/km)	Less than acceptable: >170

Table 4-20. MRI RESULTS OF CONVENTIONAL AND INVERTED SECTIONS.

Profiler Pattern	*Inverted*		*Conventional*		*Difference (%)*
	Averaged MRI (in/mi)	Condition	Averaged MRI (in/mi)	Condition	
South LN 1	54.18	Very Good	63.16	Good	16.57
North LN 1	53.36	Very Good	53.54	Very Good	0.34
South LN 2	59.98	Very Good	57.74	Very Good	-3.73
North LN 2	78.73	Good	75.39	Good	-4.24

4.9 Cost Analysis Using Pavement ME Design

4.9.1 Pavement life prediction

Comprehensive analysis of the design documents, Ground Penetrating Radar (GPR) scanning, Falling Weight Deflectometer (FWD) measurements, and coring tests mentioned in the subsections helps the research team identify appropriate inputs for Pavement ME software to ensure accurate predictions and analysis. The data selection for this study was meticulously verified to ensure the accuracy of current conditions concerning the design specifications. GPR and field coring were employed to determine the consistency of the thickness of constructed layers with the design documentation. The compatibility of GPR results and coring measurements with the design thicknesses allowed the research team to proceed confidently to subsequent stages, including back-calculation, performance prediction, and economic analysis, within the design parameters. The FWD testing and laboratory tests for resilient modulus were crucial in validating the back-calculated modulus values. These tests were designed to assess the impact of aging and traffic loading on the pavement. Two distinct FWD tests were carried out: one before applying the paving surface and another after a year of traffic exposure. The choice to use back-calculated resilient modulus was based on the completed pavement sections. Consistency between the two FWD tests provided a robust basis for analysis.

The research team synthesized these findings to conduct performance predictions and a cost-benefit evaluation using AASHTOWare ME Design software. The analyses yielded predictions for the IRI, rutting depth, AC bottom-up cracking, and thermal cracking for conventional and inverted sections, illustrated in Figure 4-8. The red lines indicate the failure criteria for different distress types. Minor differences are found between levels of distress of conventional and inverted sections except thermal cracking. The predictions of IRI, rutting depth, and AC bottom-up cracking show that the performance of both inverted and conventional sections was in great condition and did not reach the failure thresholds. The comparative performance metrics between conventional and inverted pavement sections suggest a slightly better performance for conventional pavement after 20 years of service. Specifically, the IRI for the conventional pavement stands at 145.6 in/mi (2305.6 mm/km), slightly lower than the inverted pavement's 148.6 in/mi (2353.1 mm/km). For rutting, the conventional section exhibits a rutting depth of 0.31 inches (7.87 mm) compared to 0.40 inches (10.20 mm) for the inverted section. Furthermore, neither pavement type has displayed significant bottom-up cracking. The conventional pavement has a total length of thermal cracking significantly lower (approximately 738.79 ft/mile (140.39 m/km)) compared to the inverted pavement (approximately 1022.85 ft/mile (194.37)) after 20-year service. The relationship between the thickness of the asphalt concrete layer and the incidence of thermal cracking is generally inversely proportional. Thicker layers of asphalt concrete tend to have a reduced occurrence of thermal cracking due to their enhanced ability to withstand temperature-induced stress (Jung and Vinson, 1994). The research team considered that both conventional and inverted sections could deliver 20 years of service without causing major failure. The following cost analysis will be based on 20 years in service for both pavement types.

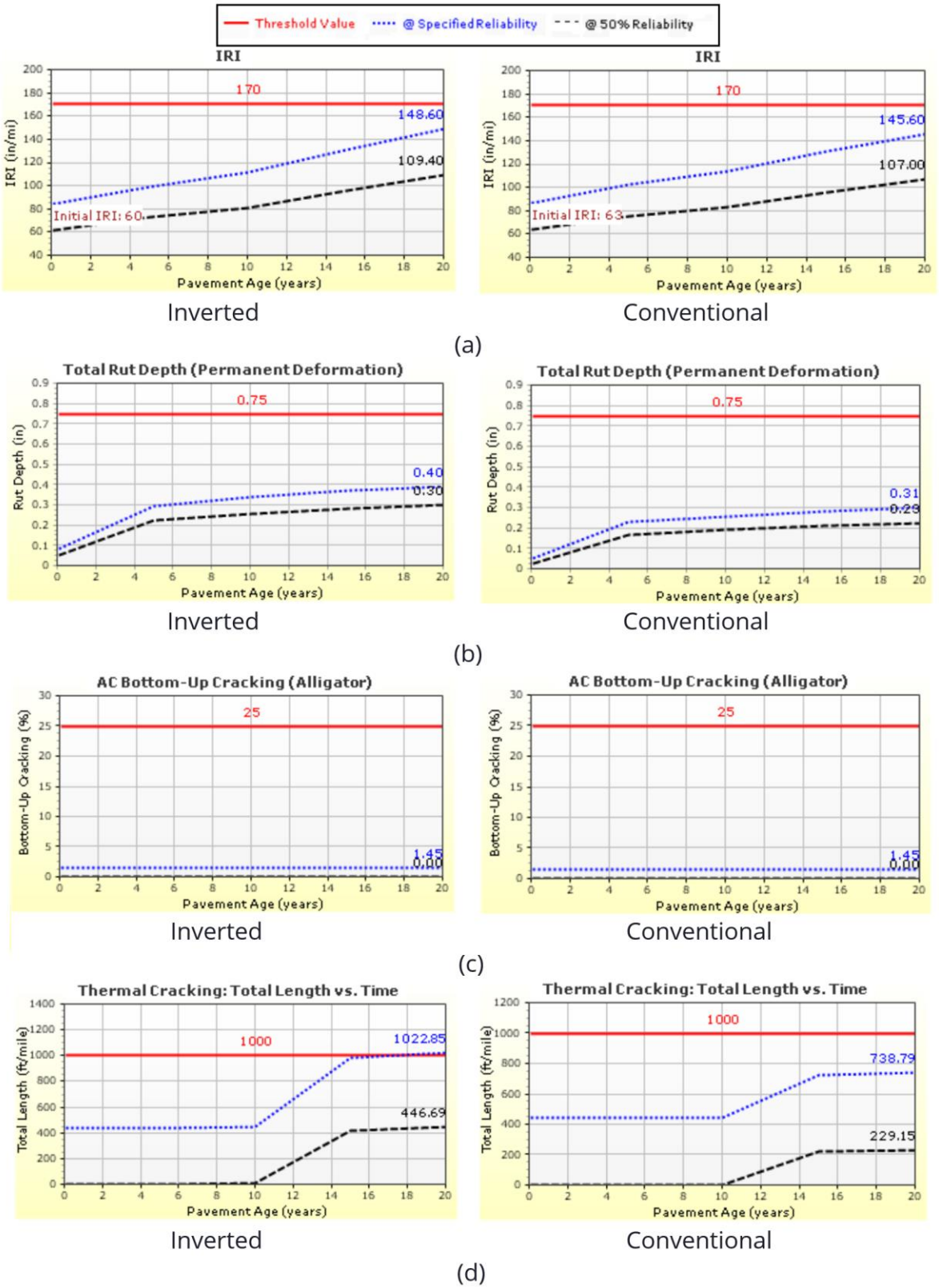

a

Figure 4-8. Predicted distress Charts: (a) IRI, (b) total rutting depth, (c) AC Bottom-up cracking, and (d) thermal cracking for inverted (left) and conventional (right) sections.

4.9.2 Cost analysis

The initial construction cost for inverted and conventional pavements varies mainly based on the price of the constituent materials used. Detailed in Table 4-21, the price of the materials was based on the local estimation. The price and quantities of materials like asphalt mixtures, aggregate, and cement for conventional and inverted pavements are converted to the cost per lane mile per inch thickness. Thus, the unit price of the AC layer is 14,677 USD per lane mile per inch thickness. The unit price of the Aggregate base layer is 20,026 USD per lane mile per inch thickness, and the CTB layer is 15,028 USD per lane mile per inch thickness. The total cost of conventional and inverted pavements per lane mile is 336,022 dollars and 291,692 dollars, respectively. Conventional pavement per lane mile cost is 15.2% higher than inverted ones. The initial cost of inverted and conventional pavements and EUAC results are summarized in Table 4-22.

The Estimated Uniform Annual Cost (EUAC) method expresses life cycle costs as an annualized cash flow estimation. The EUAC values of testing pavements can be calculated using Equation (4). The discount rate (%) is 4%, and the service life is 20 years for both inverted and conventional pavement based on the prediction results by Pavement ME. The EUAC serves as a key metric for comparing inverted versus conventional pavements economically. Through cost analysis, the EUAC for inverted pavements is determined to be 21,591 US dollars, compared to 24,725 US dollars for conventional pavements, reflecting a 14.52% cost saving. This indicates that the test inverted pavement is more cost-efficient than the conventional pavement section under similar pavement performance. It is worth noting that the thickness of the AC layer for the inverted pavement section is only one-fourth of the AC thickness of the conventional one.

Table 4-21. MATERIAL COST OF TESTING PAVEMENTS.

Layer	*Materials*	*Weight (%)*	*Unit Price (USD/kg)*	*Price (USD/lane mile)*	*Total cost (USD/lane mile)*
AC layer (per inch)	D rock	9.4	0.03	2009.7	14,677
	Manufactured Sand	47.0	0.01	622.9	
	#10	23.5	0.03	4019.4	
	Natural Sand	14.1	0.01	207.6	
	Asphalt	6.0	0.50	7817.7	
UAB layer (per inch)	Aggregate	100.0	0.03	20025.7	20,026
CTB layer (per inch)	Cement	4.0	0.02	2146.9	15,028
	Aggregate	96.0	0.05	12881.1	

Table 4-22. COST ANALYSIS OF TESTING PAVEMENTS.

Pavements		*AC*	*Aggregate Base*	*CTB*	*Total Cost (USD/lane mile)*	*EUAC*
Inverted	Layer thickness (inch)	2.25	7	8	291,692	21,591
	Cost per lane mile per inch thickness	14,677	20,026	15,028		
	Layer cost	33,023	140,182	120,224		
Conventional	Layer thickness (inch)	9.25	10	-	336,022	24,725
	Cost per lane mile per inch thickness	14,677	20,026	-		
	Layer cost	135,762	200,260	-		

Chapter 5 Conclusion

This project comprehensively involved the whole process from the construction to the in-service phase of the inverted pavement test section in Chattanooga. The goal was to thoroughly demonstrate the performance and cost-benefits of the inverted pavement structure to justify its broader implementation across the state. The study conducted detailed comparisons of the performance of inverted sections against conventional sections under identical traffic and environmental conditions.

No significant distresses have emerged, given the short observation and in-service period for the test pavement sections. The research team employed the AASHTOWare Pavement ME software to forecast the long-term performance of both inverted and conventional pavement sections. This predictive analysis was complemented by a detailed cost comparison. To ensure the accuracy and reliability of these predictions and cost evaluations, the team conducted a thorough evaluation process on the test pavement sections. This process included a critical review of initial design documents, advanced diagnostics with Ground Penetration Radar (GPR), assessments of pavement structural integrity via Falling Weight Deflectometer (FWD) tests, and direct examination of pavement core samples. These comprehensive methods provided a solid foundation for the predictive models and financial analyses.

The Mean Roughness Index (MRI) evaluations indicated that both inverted and conventional pavement sections exhibited good surface smoothness. Three inverted sections received a "Very Good" rating, and one was deemed "Good." Conversely, among conventional pavements, two sections were rated "Good," with the remaining receiving a "Very Good" rating. Also, conventional pavements exhibited greater variability in smoothness, suggesting that inverted pavements might more consistently maintain surface roughness under various traffic conditions.

Based on solid input data from the Chattanooga test pavements, the AASHTOWare ME Design software predicted minor performance differences between inverted and conventional pavements. The predicted International Roughness Index (IRI), rutting depth, and bottom-up cracking remained within acceptable limits and did not approach failure thresholds for 20 years. The conventional pavement had substantially less thermal cracking than inverted pavement because thicker asphalt layers can lessen thermal cracking. Both pavement types are expected to last 20 years without significant failure. It's significant to highlight that the asphalt concrete (AC) layer thickness in inverted pavements is merely one-fourth that of traditional conventional pavements. Through cost analysis, the Estimated Uniform Annual Cost (EUAC) for inverted pavements was determined to be $21,591, compared to $24,725 for conventional pavements, reflecting a 14.52% cost saving. This demonstrates that the test inverted pavement is more cost-efficient than the conventional pavement section under similar performance conditions.

The following are several recommendations for further research and implementation of inverted pavement technologies:

- Chattanooga Inverted pavement section had demonstrated equivalent performance to conventional pavement, suggesting it as a viable alternative.

- It is recommended that TDOT and research teams maintain ongoing collaboration for thorough performance assessments, especially as the pavement age and potential distress become more apparent. Consistent and detailed monitoring is crucial to collecting reliable data on both pavement types, facilitating accurate cost-benefit analyses, and advocating for the broader adoption of inverted pavement technology in Tennessee.
- To support carbon neutrality, a comparative carbon footprint analysis between conventional and inverted pavements is essential, given the potential for emissions reduction through thinner asphalt layers in inverted pavements.
- Enhanced inverted pavement performance can be achieved through detailed design and sensitivity analysis focused on cost, benefits, and carbon footprint. Optimizing design, materials, and structure configuration is crucial for maximizing performance and supporting statewide implementation.

References

1. [software] Retrieved from: https://me-design.com/MEDesign/
2. [website] Retrieved from: https://me-design.com/medesign/ClimaticData.html
3. Baghel, R.S., Reddy, K.S. and Chandrappa, A.K., 2021. Comparison of inverted pavements with different types of crack relief layers. In 2021 International Airfield and Highway Pavements Conference, Rosemont.
4. BAKFAA v3.4 manual, retrieved from https://www.airporttech.tc.faa.gov/Products/Airport-Safety-Papers-Publications/Airport-Safety-Detail/ArtMID/3682/ArticleID/11/BAKFAA-330
5. Biswal, D.R., Chandra Sahoo, U. and Ranjan Dash, S., 2020. Structural response of an inverted pavement with stabilised base by numerical approach considering isotropic and anisotropic properties of unbound layers. Road Materials and Pavement Design, 21(8), pp.2160-2179.
6. C. Chang, D. Saenz, S. Nazarian, I.N. Abdallah, A. Wimsatt, T. Freeman, E.G. Fernando, TxDOT Guidelines to Assign PMIS Treatment Levels, 2014.
7. C. Plati, A. Loizos, K. Gkyrtis, Assessment of Modern Roadways Using Non-destructive Geophysical Surveying Techniques, Springer Netherlands, 2020. doi:10.1007/s10712-019-09518-y.
8. Cortes DD, Santamarina JC. The LaGrange case history: Inverted pavement system characterisation and preliminary numerical analyses. Int J Pavement Eng 2013;14: 463–71. https://doi.org/10.1080/10298436.2012.742192.
9. Cortes, D.D. and Santamarina, J.C., 2013. The LaGrange case history: inverted pavement system characterisation and preliminary numerical analyses. International Journal of Pavement Engineering, 14(5), pp.463-471.
10. De Almeida, D.C., 2021. Performance evaluation of inverted pavements: comparative analysis of South African and Brazilian experiences (Doctoral dissertation, University of Pretoria).
11. Donovan, Sean. (2022). Performance evaluation of inverted pavement structures. Thesis. Georgia Tech Digital Repository. http://hdl.handle.net/1853/70184
12. Efthymios Papadopoulos and Juan Carlos Santamarina, Inverted base pavements: construction and performance, International Journal of Pavement Engineering, Volume 20, 2019, Pg 697-703, https://doi.org/10.1080/10298436.2017.1326237
13. Federal Highway Administration. 1999 Status of the Nation's Highways, Bridges, and Transit: Conditions and Performance, Report to Congress. Federal Highway Administration. Report FHWA-PL-08-017. Washington D.C., May 2001. Available on-line at: http://www.fhwa.dot.gov////policy/1999cpr/index.htm. Accessed August 1, 2002.
14. Ghanizadeh, A.R., Ghaderi, F. and Tavassoti, P., 2022. Numerical investigation of the performance of geocell-reinforced granular base in inverted pavement systems using nonlinear finite element modeling. Canadian Journal of Civil Engineering, 50(5), pp.395-407.
15. GSSI RADAN 7 [software]. Retrieved from https://www.geophysical.com/support#filter=.software

16. Horak, E., Emery, S., and Maina, Review of Falling Weight Deflectometer Deflection Benchmark Analysis on Roads and Airfields, in: Conf. Asph. Pavement South Africa, Sun City, South Africa, 2015.
17. International Roughness Index. Web page from the Road Roughness Home Page: http://www.umtri.umich.edu/erd/roughness/iri.html). Accessed 4 October 2001.
18. Jiang Xi, Gabrielson Jay, Titi Hani, Huang Baoshan, Bai Yun, Polaczyk Pawel, Hu Wei, Zhang Miaomiao, Xiao Rui, Field investigation and numerical analysis of an inverted pavement system in Tennessee, USA, Transportation Geotechnics, Volume 35, 2022, 100759, ISSN 2214-3912, https://doi.org/10.1016/j.trgeo.2022.100759.9.
19. Jiang, X., Gabrielson, J., Titi, H., Huang, B., Bai, Y., Polaczyk, P., Hu, W., Zhang, M. and Xiao, R., 2022. Field investigation and numerical analysis of an inverted pavement system in Tennessee, USA. Transportation Geotechnics, 35, p.100759.
20. Jiang, X., Huang, B., Titi, H. and Polaczyk, P., 2022. Evaluating the Performance of Inverted Pavements in Tennessee (No. RES 2020-12). Tennessee. Department of Transportation.
21. Jiang, X., Zhang, F., Huang, B., Titi, H., Polaczyk, P., Ma, Y., Wang, Y. and Cheng, Z., 2024. Full-scale accelerated testing of geogrid-reinforced inverted pavements. Geotextiles and Geomembranes.
22. Jiang, X., Zhang, M., Xiao, R., Polaczyk, P., Bai, Y. and Huang, B., 2021. An investigation of structural responses of inverted pavements by numerical approaches considering nonlinear stress-dependent properties of unbound aggregate layer. Construction and Building Materials, 303, p.124505.
23. Jol, H.M. ed., 2008. Ground penetrating radar theory and applications. elsevier.
24. Jung, D.H. and Vinson, T.S., 1994. Low-temperature cracking: Test selection (No. SHRP-A-400).
25. K.R. Maser, T. Scullion, Automated Pavement Subsurface Profiling Using Radar: Case Studies of Four Experimental Field Sites, Transp. Res. Rec. 1344 (1992) 148–154.
26. K.R. Maser, T. Scullion, Automated Pavement Subsurface Profiling Using Radar: Case Studies of Four Experimental Field Sites, Transp. Res. Rec. 1344 (1992) 148–154.
27. Khan, S., Nagabhushana, M.N., Hossain, K., Tiwari, D., Guruvittal, U.K. and Bazan, C., 2022. Performance evaluation of fly ash–based inverted pavement system. Journal of Transportation Engineering, Part B: Pavements, 148(2), p.04022028.
28. Khan, Shahbaz & Nagabhushana, M.N. & Tiwari, Devesh. (2020). Performance Evaluation of Inverted Pavement - A Review.
29. Khare, P., Machesky, J., Soto, R., He, M., Presto, A.A. and Gentner, D.R., 2020. Asphalt-related emissions are a major missing nontraditional source of secondary organic aerosol precursors. Science advances, 6(36), p.eabb9785.
30. Lewis DE, Jared DM. Construction and Performance of Inverted Pavements in Georgia. Transp Res Board 91st Annu Meet 2012.
31. Md Yusoff, Nur Izzi & Hardwiyono, Sentot & Ismail, Norfarah Nadia & Taha, Mohd & Rosyidi, Sri Atmaja P. & Nayan, Khairul. (2015). Measurements of the Elastic Modulus of Pavement Subgrade Layers Using the SASW and FWD Test Methods. The Baltic Journal of Road and Bridge Engineering. 10(2):174-181.
32. Papadopoulos, E. and Santamarina, J.C., 2016. Analysis of inverted base pavements with thin-asphalt layers. International Journal of Pavement Engineering, 17(7), pp.590-601.

33. Papadopoulos, E. and Santamarina, J.C., 2019. Inverted base pavements: construction and performance. International Journal of Pavement Engineering, 20(6), pp.697-703.
34. Papadopoulos, Efthymios & Santamarina, J.. (2015). Analysis of inverted base pavements with thin-asphalt layers. International Journal of Pavement Engineering. 17. 1-12. 10.1080/10298436.2015.1007232.
35. Plati, C., 2019. Sustainability factors in pavement materials, design, and preservation strategies: A literature review. Construction and Building Materials, 211, pp.539-555.
36. U.S. Department of Transportation, LOUISIANA EXPERIENCE WITH INVERTED PAVEMENT SYSTEMS LOUISIANA EXPERIENCE WITH FHWA-HIF-19-082, 2017. https://www.fhwa.dot.gov/pavement/sustainability/case_studies/hif19082.pdf.
37. Witczak, M.W., Kaloush, K., Pellinen, T., Basyouny, M.E., and Quintus, H.V., "Simple Performance Test for Superpave Mix Design," NCHRP Report No. 465, 2002.

Appendices

Appendix A: Data input of AASHTOWare Pavement ME Design

1. Conventional sections

Layer Information

Layer 1 Flexible : Default asphalt concrete

Asphalt		
Thickness (in)	9.3	
Unit weight (pcf)	150.0	
Poisson's ratio	Is Calculated?	False
	Ratio	0.35
	Parameter A	-
	Parameter B	-

Asphalt Dynamic Modulus (Input Level: 3)

Gradation	Percent Passing
3/4-inch sieve	100
3/8-inch sieve	100
No.4 sieve	92
No.200 sieve	7.2

Asphalt Binder

Parameter	Value
Grade	Superpave Performance Grade
Binder Type	70-22
A	10.299
VTS	-3.426

General Info

Name	Value
Reference temperature (ºF)	70
Effective binder content (%)	11.6
Air voids (%)	7
Thermal conductivity (BTU/hr-ft-ºF)	0.67
Heat capacity (BTU/lb-ºF)	0.23
Asphalt content by weight (%)	6
Aggregate parameter	0.3685

Identifiers

Field	Value
Display name/identifier	Default asphalt concrete
Description of object	
Author	
Date Created	10/30/2010 1:00:00 AM
Approver	
Date approved	10/30/2010 1:00:00 AM
State	
District	
County	
Highway	
Direction of Travel	
From station (miles)	
To station (miles)	
Province	
User defined field 1	
User defined field 2	
User defined field 3	
Revision Number	0

Figure A-1. Layer information of the Surface layer of the conventional sections

Layer 2 Non-stabilized Base : Permeable aggregate

Unbound	
Layer thickness (in)	10.0
Poisson's ratio	0.35
Coefficient of lateral earth pressure (k0)	0.5

Modulus (Input Level: 2)

Analysis Type:	Modify input values by temperature/moisture
Method:	Resilient Modulus (psi)

Resilient Modulus (psi)
100000.0

Use Correction factor for NDT modulus?	-
NDT Correction Factor:	-

Identifiers

Field	Value
Display name/identifier	Permeable aggregate
Description of object	Default material
Author	AASHTO
Date Created	1/1/2011 12:00:00 AM
Approver	
Date approved	1/1/2011 12:00:00 AM
State	
District	
County	
Highway	
Direction of Travel	
From station (miles)	
To station (miles)	
Province	
User defined field 1	
User defined field 2	
User defined field 3	
Revision Number	0

Sieve

Liquid Limit	6.0
Plasticity Index	1.0
Is layer compacted?	True

	Is User Defined?	Value
Maximum dry unit weight (pcf)	False	123.6
Saturated hydraulic conductivity (ft/hr)	False	3.666e-03
Specific gravity of solids	False	2.7
Water Content (%)	False	9.4

User-defined Soil Water Characteristic Curve (SWCC)	
Is User Defined?	False
af	3.9340
bf	2.6076
cf	0.7931
hr	114.4000

Sieve Size	% Passing
0.001mm	
0.002mm	
0.020mm	
#200	7.2
#100	13.1
#80	
#60	
#50	
#40	
#30	39.0
#20	
#16	
#10	
#8	73.0
#4	92.0
3/8-in.	100.0
1/2-in.	
3/4-in.	
1-in.	
1 1/2-in.	
2-in.	
2 1/2-in.	
3-in.	
3 1/2-in.	

Figure A-2. Layer information of the Base layer of the conventional sections

Layer 3 Subgrade : A-4

Unbound	
Layer thickness (in)	Semi-infinite
Poisson's ratio	0.35
Coefficient of lateral earth pressure (k0)	0.5

Modulus (Input Level: 2)

Analysis Type:	Modify input values by temperature/moisture
Method:	Resilient Modulus (psi)

Resilient Modulus (psi)
45000.0

Use Correction factor for NDT modulus?	-
NDT Correction Factor:	-

Identifiers

Field	Value
Display name/identifier	A-4
Description of object	Default material
Author	AASHTO
Date Created	1/1/2011 12:00:00 AM
Approver	
Date approved	1/1/2011 12:00:00 AM
State	
District	
County	
Highway	
Direction of Travel	
From station (miles)	
To station (miles)	
Province	
User defined field 1	
User defined field 2	
User defined field 3	
Revision Number	0

Sieve

Liquid Limit	21.0
Plasticity Index	5.0
Is layer compacted?	True

	Is User Defined?	Value
Maximum dry unit weight (pcf)	False	119
Saturated hydraulic conductivity (ft/hr)	False	7.589e-06
Specific gravity of solids	False	2.7
Water Content (%)	False	11.8

User-defined Soil Water Characteristic Curve (SWCC)	
Is User Defined?	False
af	68.8377
bf	0.9983
cf	0.4757
hr	500.0000

Sieve Size	% Passing
0.001mm	
0.002mm	
0.020mm	
#200	60.6
#100	
#80	73.9
#60	
#50	
#40	82.7
#30	
#20	
#16	
#10	89.9
#8	
#4	93.0
3/8-in.	95.6
1/2-in.	96.7
3/4-in.	98.0
1-in.	98.7
1 1/2-in.	99.4
2-in.	99.6
2 1/2-in.	
3-in.	
3 1/2-in.	99.8

Figure A-3. Layer information of the Subgrade layer of the conventional sections.

Calibration Coefficients

AC Fatigue

$$N_f = 0.00432 * C * \beta_{f1} k_1 \left(\frac{1}{\varepsilon_1}\right)^{k_2 \beta_{f2}} \left(\frac{1}{E}\right)^{k_3 \beta_{f3}}$$

$$C = 10^M$$

$$M = 4.84\left(\frac{V_b}{V_a + V_b} - 0.69\right)$$

k1: 3.75	
k2: 2.87	
k3: 1.46	
Bf1: (5.014 * Pow(hac,-3.416)) * 1 + 0	
Bf2: 1.38	
Bf3: 0.88	

AC Rutting

$$\frac{\varepsilon_p}{\varepsilon_r} = k_z \beta_{r1} 10^{k_1} T^{k_2 \beta_{r2}} N^{k_3 \beta_{r3}}$$

$$k_z = (C_1 + C_2 * depth) * 0.328196^{depth}$$

$$C_1 = -0.1039 * H_\alpha^2 + 2.4868 * H_\alpha - 17.342$$

$$C_2 = 0.0172 * H_\alpha^2 - 1.7331 * H_\alpha + 27.428$$

Where:

$H_{ac} = total\ AC\ thickness(in)$

$\varepsilon_p = plastic\ strain\left(^{in}/_{in}\right)$

$\varepsilon_r = resilient\ strain\left(^{in}/_{in}\right)$

$T = layer\ temperature\left(^{\circ}F\right)$

$N = number\ of\ load\ repetitions$

acRuttingStandardDeviation	0.24 * Pow(RUT,0.8026) + 0.001	
AC Layer 1	K1:-2.45 K2:3.01 K3:0.22	Br1:0.4 Br2:0.52 Br3:1.36

Thermal Fracture

$$C_f = \beta_{t1} N\left[\frac{1}{\sigma_d} log\left(\frac{C}{h_{AC}}\right)\right]$$

$$\Delta C = A(\Delta K)^n$$

$$A = k_t \beta_t 10^{[4.389 - 2.52 \log(E_{HMA} \sigma_m n)]}$$

Cf = Observed amount of thermal cracking, ft. / 500ft.
β_{t1} = Regression coefficient determined through global calibration (400)
N[z] = Standard normal distribution evaluated at [z]
σ_d = Standard deviation of the logarithm of crack depth in the pavement (0.769), in.
C = Crack depth, in.
h_{AC} = Thickness of asphalt layer, in.
ΔC = Change in the crack depth due to a cooling cycle
ΔK = Change in the stress intensity factor due to a cooling cycle
A, n = Fracture parameters for the asphalt mixture
E = Asphalt mixture stiffness, MPa
σ_m = Undamaged mixture tensile strength, MPa
k_t = Regression coefficient determined through field calibration
β_t = Calibration parameter

Level 1 K: (0.13 * Pow(MAAT,2) - 11.68 * MAAT + 244.14) * 1 + 0	Level 1 Standard Deviation: 0.14 * THERMAL + 343
Level 2 K: (0.13 * Pow(MAAT,2) - 11.68 * MAAT + 244.14) * 1 + 0	Level 2 Standard Deviation: 0.20 * THERMAL + 343
Level 3 K: (0.13 * Pow(MAAT,2) - 11.68 * MAAT + 244.14) * 1 + 0	Level 3 Standard Deviation: 0.2386 * THERMAL + 343

CSM Fatigue

$$N_f = 10^{\left(\frac{k_1 \beta_{c1}\left(\frac{\sigma_s}{M_r}\right)}{k_2 \beta_{c2}}\right)}$$

$N_f = number\ of\ repetitions\ to\ fatigue\ cracking$

$\sigma_s = Tensile\ stress(psi)$

$M_r = modulus\ of\ rupture(psi)$

k1: 0.972	k2: 0.0825	Bc1: 1	Bc2:1

Figure A-4. Calibration coefficients used for conventional section calculations (part 1).

Unbound Layer Rutting

$$\delta_a(N) = \beta_{s_1} k_1 \varepsilon_v h \left(\frac{\varepsilon_0}{\varepsilon_r}\right) \left| e^{-\left(\frac{\rho}{N}\right)^{\beta}} \right|$$

$\delta_a = permanent\ deformation\ for\ the\ layer$
$N = number\ of\ repetitions$
$\varepsilon_v = average\ veritcal\ strain(in/in)$
$\varepsilon_0, \beta, \rho = material\ properties$
$\varepsilon_r = resilient\ strain(in/in)$

Base Rutting		Subgrade Rutting	
k1: 0.965	Bs1: 1	k1: 0.965	Bs1: 1
Standard Deviation (BASERUT) 0.1477 * Pow(BASERUT,0.6711) + 0.001		Standard Deviation (BASERUT) 0.1235 * Pow(SUBRUT,0.5012) + 0.001	

AC Cracking

AC Top Down Cracking

$$L(t) = L_{Max} e^{-\left(\frac{C_1 \rho}{t - C_3 t_0}\right)^{C_2 \beta}}$$

$$t_0(\text{Days}) = \frac{k_{L1}}{1 + e^{(k_{L2} \times 100 \times a_0/2A_0) + (k_{L3} \times HT) + (k_{L4} \times LT) + (k_{L5} \times \log_{10} AADTT)}}$$

c1: 2.5219	c2: 0.8069	c3: 1

kL1: 64271618	kL2: 0.2855	kL3: 0.011
kL4: 0.01488	kL5: 3.266	

acCrackingTopStandardDeviation

0.3657 * TOP + 3.6563

AC Bottom Up Cracking

$$FC = \left(\frac{6000}{1 + e^{\left(C_1 * C_1' + C_2 * C_2' \log_{10}(D * 100)\right)}}\right) * \left(\frac{1}{60}\right)$$

$$C_2' = -2.40874 - 39.748 * (1 + h_{ac})^{-2.856}$$

$$C_1' = -2 * C_2'$$

c1: 1.31	c2: (0.867 + 0.2583 * hac) * 1 + 0	c3: 6000

acCrackingBottomStandardDeviation

1.13 + 13/(1+exp(7.57-15.5*LOG10(BOTTOM+0.0001)))

CSM Cracking

$$FC_{ctb} = C_1 + \frac{C_2}{1 + e^{C_3 - C_4 * \log_{10}(Damage)}}$$

C1: 0	C2: 75	C3: 2	C4: 2

csmCrackingStandardDeviation

CTB*1

IRI Flexible Pavements

C1 - Rutting
C2 - Fatigue Crack
C3 - Transverse Crack
C4 - Site Factors

C1: 40	C2: 0.4	C3: 0.008	C4: 0.015

Figure A-5. Calibration coefficients used for conventional section calculations (part 2).

2. Inverted section

Layer Information

Layer 1 Flexible : Default asphalt concrete

Asphalt		
Thickness (in)	2.3	
Unit weight (pcf)	150.0	
Poisson's ratio	Is Calculated?	False
	Ratio	0.35
	Parameter A	-
	Parameter B	-

Asphalt Dynamic Modulus (Input Level: 3)

Gradation	Percent Passing
3/4-inch sieve	100
3/8-inch sieve	100
No.4 sieve	92
No.200 sieve	7.2

Asphalt Binder

Parameter	Value
Grade	Superpave Performance Grade
Binder Type	64-22
A	10.98
VTS	-3.68

General Info

Name	Value
Reference temperature (ºF)	70
Effective binder content (%)	11.6
Air voids (%)	7
Thermal conductivity (BTU/hr-ft-ºF)	0.67
Heat capacity (BTU/lb-ºF)	0.23
Asphalt content by weight (%)	6
Aggregate parameter	0.3685

Identifiers

Field	Value
Display name/identifier	Default asphalt concrete
Description of object	
Author	
Date Created	10/30/2010 1:00:00 AM
Approver	
Date approved	10/30/2010 1:00:00 AM
State	
District	
County	
Highway	
Direction of Travel	
From station (miles)	
To station (miles)	
Province	
User defined field 1	
User defined field 2	
User defined field 3	
Revision Number	0

Figure A-6. Layer information of the Surface layer of the inverted section.

Layer 2 Non-stabilized Base : Permeable aggregate

Unbound	
Layer thickness (in)	7.0
Poisson's ratio	0.35
Coefficient of lateral earth pressure (k0)	0.5

Modulus (Input Level: 2)

Analysis Type:	Modify input values by temperature/moisture
Method:	Resilient Modulus (psi)

Resilient Modulus (psi)
100000.0

Use Correction factor for NDT modulus?	-
NDT Correction Factor:	-

Identifiers

Field	Value
Display name/identifier	Permeable aggregate
Description of object	Default material
Author	AASHTO
Date Created	1/1/2011 12:00:00 AM
Approver	
Date approved	1/1/2011 12:00:00 AM
State	
District	
County	
Highway	
Direction of Travel	
From station (miles)	
To station (miles)	
Province	
User defined field 1	
User defined field 2	
User defined field 3	
Revision Number	0

Sieve

Liquid Limit	6.0
Plasticity Index	1.0
Is layer compacted?	True

	Is User Defined?	Value
Maximum dry unit weight (pcf)	False	123.6
Saturated hydraulic conductivity (ft/hr)	False	3.666e-03
Specific gravity of solids	False	2.7
Water Content (%)	False	9.4

User-defined Soil Water Characteristic Curve (SWCC)	
Is User Defined?	False
af	3.9340
bf	2.6076
cf	0.7931
hr	114.4000

Sieve Size	% Passing
0.001mm	
0.002mm	
0.020mm	
#200	7.2
#100	13.1
#80	
#60	
#50	
#40	
#30	39.0
#20	
#16	
#10	
#8	73.0
#4	92.0
3/8-in.	100.0
1/2-in.	
3/4-in.	
1-in.	
1 1/2-in.	
2-in.	
2 1/2-in.	
3-in.	
3 1/2-in.	

Figure A-7. Layer information of the Base layer of the inverted section.

Layer 3 Subgrade : A-4

Unbound	
Layer thickness (in)	Semi-infinite
Poisson's ratio	0.35
Coefficient of lateral earth pressure (k0)	0.5

Modulus (Input Level: 2)

Analysis Type:	Modify input values by temperature/moisture
Method:	Resilient Modulus (psi)

Resilient Modulus (psi)
50000.0

Use Correction factor for NDT modulus?	-
NDT Correction Factor:	-

Identifiers

Field	Value
Display name/identifier	A-4
Description of object	Default material
Author	AASHTO
Date Created	1/1/2011 12:00:00 AM
Approver	
Date approved	1/1/2011 12:00:00 AM
State	
District	
County	
Highway	
Direction of Travel	
From station (miles)	
To station (miles)	
Province	
User defined field 1	
User defined field 2	
User defined field 3	
Revision Number	0

Sieve

Liquid Limit	21.0
Plasticity Index	5.0
Is layer compacted?	True

	Is User Defined?	Value
Maximum dry unit weight (pcf)	False	119
Saturated hydraulic conductivity (ft/hr)	False	7.589e-06
Specific gravity of solids	False	2.7
Water Content (%)	False	11.8

User-defined Soil Water Characteristic Curve (SWCC)	
Is User Defined?	False
af	68.8377
bf	0.9983
cf	0.4757
hr	500.0000

Sieve Size	% Passing
0.001mm	
0.002mm	
0.020mm	
#200	60.6
#100	
#80	73.9
#60	
#50	
#40	82.7
#30	
#20	
#16	
#10	89.9
#8	
#4	93.0
3/8-in.	95.6
1/2-in.	96.7
3/4-in.	98.0
1-in.	98.7
1 1/2-in.	99.4
2-in.	99.6
2 1/2-in.	
3-in.	
3 1/2-in.	99.8

Figure A-8. Layer information of the Subgrade layer of the inverted section.

Calibration Coefficients

AC Fatigue	
$N_f = 0.00432 * C * \beta_{f1} k_1 \left(\frac{1}{\varepsilon_1}\right)^{k_2 \beta_{f2}} \left(\frac{1}{E}\right)^{k_3 \beta_{f3}}$	k1: 3.75
	k2: 2.87
	k3: 1.46
$C = 10^M$	Bf1: 0.02054
$M = 4.84\left(\frac{V_b}{V_a + V_b} - 0.69\right)$	Bf2: 1.38
	Bf3: 0.88

AC Rutting		
$\frac{\varepsilon_p}{\varepsilon_r} = k_z \beta_{r1} 10^{k_1} T^{k_2 \beta_{r2}} N^{k_3 \beta_{r3}}$ $k_z = (C_1 + C_2 * depth) * 0.328196^{depth}$ $C_1 = -0.1039 * H_{ac}^2 + 2.4868 * H_{ac} - 17.342$ $C_2 = 0.0172 * H_{ac}^2 - 1.7331 * H_{ac} + 27.428$ *Where:* $H_{ac} = total\ AC\ thickness(in)$	$\varepsilon_p = plastic\ strain\left(^{in}/_{in}\right)$ $\varepsilon_r = resilient\ strain\left(^{in}/_{in}\right)$ $T = layer\ temperature(^{\circ}F)$ $N = number\ of\ load\ repetitions$	
acRuttingStandardDeviation	0.24 * Pow(RUT,0.8026) + 0.001	
AC Layer 1	K1:-2.45 K2:3.01 K3:0.22	Br1:0.4 Br2:0.52 Br3:1.36

Thermal Fracture		
$C_f = \beta_{t1} N\left[\frac{1}{\sigma_d} log\left(\frac{C}{h_{AC}}\right)\right]$ $\Delta C = A(\Delta K)^n$ $A = k_t \beta_t 10^{[4.389 - 2.52 \log(E_{HMA} \sigma_m n)]}$	*Cf = Observed amount of thermal cracking, ft. / 500ft.* *β_{t1} = Regression coefficient determined through global calibration (400)* *N[z] = Standard normal distribution evaluated at [z]* *σ_d = Standard deviation of the logarithm of crack depth in the pavement (0.769), in.* *C = Crack depth, in.* *h_{AC} = Thickness of asphalt layer, in.* *ΔC = Change in the crack depth due to a cooling cycle* *ΔK = Change in the stress intensity factor due to a cooling cycle* *A, n = Fracture parameters for the asphalt mixture* *E = Asphalt mixture stiffness, MPa* *σ_m = Undamaged mixture tensile strength, MPa* *k_t = Regression coefficient determined through field calibration* *β_t = Calibration parameter*	
Level 1 K: (0.13 * Pow(MAAT,2) - 11.68 * MAAT + 244.14) * 1 + 0		Level 1 Standard Deviation: 0.14 * THERMAL + 343
Level 2 K: (0.13 * Pow(MAAT,2) - 11.68 * MAAT + 244.14) * 1 + 0		Level 2 Standard Deviation: 0.20 * THERMAL + 343
Level 3 K: (0.13 * Pow(MAAT,2) - 11.68 * MAAT + 244.14) * 1 + 0		Level 3 Standard Deviation: 0.2386 * THERMAL + 343

CSM Fatigue			
$N_f = 10^{\left(\frac{k_1 \beta_{c1} \left(\frac{\sigma_s}{M_r}\right)}{k_2 \beta_{c2}}\right)}$	$N_f = number\ of\ repetitions\ to\ fatigue\ cracking$ $\sigma_s = Tensile\ stress(psi)$ $M_r = modulus\ of\ rupture(psi)$		
k1: 0.972	k2: 0.0825	Bc1: 1	Bc2:1

Figure A-9. Calibration coefficients used for inverted section calculations.